

Topological Structure of the SU(3) Vacuum

UKQCD Collaboration

Douglas A. Smith¹ and Michael J. Teper²

¹Department of Physics, University of Edinburgh,
Mayfield Road, Edinburgh EH9 3JZ, U.K.

²Theoretical Physics, University of Oxford,
1 Keble Road, Oxford, OX1 3NP, U.K.

Abstract

We investigate the topological structure of the vacuum in SU(3) lattice gauge theory. We use under-relaxed cooling to remove the high-frequency fluctuations and a variety of “filters” to identify the topological charges in the resulting smoothed field configurations. We find a densely packed vacuum with an average instanton size, in the continuum limit, of $\bar{\rho} \sim 0.5$ fm. The density at large ρ decreases rapidly as $1/\rho^{11}$. At small sizes we see some signs of a trend towards the asymptotic perturbative behaviour of $D(\rho) \propto \rho^6$. We find that an interesting polarisation phenomenon occurs: the large topological charges tend to have, on the average, the same sign and are over-screened by the smaller charges which tend to have, again on the average, the opposite sign to the larger instantons. We also calculate the topological susceptibility, χ_t , for which we obtain a continuum value of $\chi_t^{1/4} \sim 187$ MeV. We perform the calculations for various volumes, lattice spacings and numbers of cooling sweeps, so as to obtain some control over the associated systematic errors. The coupling range is $6.0 \leq \beta \leq 6.4$ and the lattice volumes range from $16^3 48$ to $32^3 64$.

1 Introduction

SU(N) gauge fields in four Euclidean dimensions possess an integer topological charge Q [1]. The topological fluctuations of the gauge fields are important in QCD; for example they are the reason why the η' has a mass $\sim 1\text{GeV}$ rather than being a Goldstone boson [2]. One can also argue that they have something to do with chiral symmetry breaking [3, 4, 5, 6] and that they may have a significant influence upon the hadron spectrum [4]. The reason why topology might be able to do all this is that an isolated instanton produces a zero-mode in the Dirac operator. In the real vacuum these modes will mix with each other and shift away from zero. Just how they do so will determine their importance for the physics described above. This mixing will be determined by the topological structure of the vacuum; and in the first instance by how large and densely packed are the component topological charges. Although what one ultimately wants to know is what happens in the vacuum of QCD, the pure SU(3) gauge theory is also interesting; not least because of its relevance to the physics of quenched QCD, which seems to be a good approximation to the real world [7]. Moreover in the case of the η' it turns out that it is the topological charge in the pure gauge theory that is most relevant: one can use large- N_c arguments [8, 9] to relate the strength of the topological fluctuations, $\langle Q^2 \rangle$, in the SU(3) gauge vacuum to $m_{\eta'}$:

$$\chi_t \equiv \frac{\langle Q^2 \rangle}{\text{volume}} \simeq \frac{f_\pi^2}{2N_f} (m_{\eta'}^2 + m_\eta^2 - 2m_K^2) \sim (180 \text{ MeV})^4. \quad (1)$$

Naturally this has long been a focus for lattice calculations [10] and indeed it appears that eqn(1) is satisfied [10, 11, 12] as well as one could expect.

In this paper we attempt to see what one can learn about the detailed topological structure of the SU(3) vacuum, using simulations of the corresponding lattice theory. Some of our initial motivation was provided by an early work of this kind [13] in the SU(2) theory. Recently, several more detailed SU(2) studies have appeared [14, 15, 16] as well as preliminary reports [17, 18, 19] of some SU(3) work (including a brief summary of the work in this paper). Most of these papers appeared too recently to influence our work. For this reason we shall not attempt to review them or to compare our results in detail with theirs. However the reader should be aware that there are some quite sharp disagreements within the most recent SU(2) calculations. In particular between those studies that claim to find a relatively dilute gas of rather small instantons, [15] and those that find a dense gas of considerably larger instantons [16]. Naively, this difference would seem to be important to the physics that one derives from the topological structure; in particular the former picture fits better with instanton liquid models [4]. This indicates that current lattice calculations of topological structure – including this one – should be regarded as exploratory.

The work we do in this paper uses an ensemble of stored SU(3) field configurations that were generated by UKQCD for other purposes. All were generated with a standard plaquette action on periodic lattices. We shall analyse 100 $16^3 48$ and 50 $32^3 64$ lattice field configurations at $\beta = 6.0$, 100 $24^3 48$ configurations at $\beta = 6.2$, and 20 $32^3 64$ configurations at $\beta = 6.4$. The field configurations are typically separated by 800 to 2400 Monte Carlo sweeps and therefore represent approximately independent snapshots of the vacuum. The lattice spacing a decreases

by almost a factor of two over our range of β and so this will allow us some control over the continuum limit of the theory. At the same time, the two quite different volumes at $\beta = 6.0$ will allow us some control over the thermodynamic limit.

In the next section we discuss topology on the lattice and introduce the cooling algorithm which we use to reveal the topological charge density, $Q(x)$. Once we have $Q(x)$, we then want to decompose it into a sum of instantons and anti-instantons of various sizes. For the densely packed vacuum that we find, this represents a difficult pattern recognition problem. We shall provide a sequence of procedures - one might call them filters - which are designed to solve this problem. These procedures are necessarily approximate and the details can be tedious, but they are essential for anyone who wishes to reproduce our calculations. For this reason we shall relegate some of the technical details to the appendix. There follow two sections describing the main results of our investigation of the vacuum topological structure. This will include the instanton size density, $D(\rho)$, with a particular emphasis on the mean instanton size, the functional form of the small- ρ tail, where asymptotic freedom makes asymptotic predictions, and the large- ρ tail, which is determined by analytically incalculable infrared effects. We then investigate the correlations between topological charges. Here we find a quite striking long-distance polarisation phenomenon which has not, as far as we are aware, been remarked upon before. The next section contains our calculation of the continuum topological susceptibility, something which is free of the many uncertainties that adhere to our calculations of the vacuum structure. We finish with some conclusions. Throughout the paper we attempt to point out how our study can and should be improved.

2 Topology of lattice gauge fields

Two continuous gauge fields that have different topological charges cannot be continuously deformed into each other. When we discretise space-time, however, the fields are no longer continuous and the notion of topology becomes ambiguous. Nonetheless, because the theory is renormalisable (and because the lattice is surely a good regulator) it must be the case that we recover all the usual topological properties as the lattice spacing vanishes, $a \rightarrow 0$. (For a brief discussion of this issue see [20].) In this section we summarise some relevant properties of continuum topology and some of the problems that arise when gauge fields are regularised onto a space-time lattice. We focus on one approach to solving these problems, ‘cooling’ [22, 10], and then motivate in some detail the particular version of cooling that we shall use in this paper.

2.1 topology of continuum fields

The topological charge, Q , of a gauge field can be expressed as the integral over Euclidean space-time of a topological charge density, $Q(x)$, where

$$Q(x) = \frac{1}{32\pi^2} \epsilon_{\mu\nu\rho\sigma} \text{Tr}\{F_{\mu\nu}(x)F_{\rho\sigma}(x)\}. \quad (2)$$

The minimum action field configuration with $Q = 1$ is the instanton. The action and topological charge density are localised within a core of size ρ . At the classical level the theory is scale invariant and so all sizes are possible and the action is independent of ρ . The gauge potential of an instanton of size ρ centered at $x = 0$ is given by

$$A_\mu^I(x) = \frac{x^2}{x^2 + \rho^2} g^{-1}(x) \partial_\mu g(x) \quad (3)$$

where

$$g(x) = \frac{x_0 + ix_j \sigma_j}{(x_\mu x_\mu)^{1/2}} \quad (4)$$

up to a gauge transformation. These expressions are for SU(2); they can be trivially extended to SU(3) by embedding the SU(2) fields into SU(3) fields.

In the semiclassical limit a field of charge Q will typically contain n_I instantons and $n_{\bar{I}} = n_I - Q$ anti-instantons, all of which are well separated. In this dilute gas approximation, the average density of instantons will depend on ρ as

$$D(\rho) d\rho = \frac{d\rho}{\rho} \frac{1}{\rho^4} e^{-\frac{8\pi^2}{g^2(\rho)}} \dots \quad (5)$$

where the ‘...’ represents factors varying weakly with ρ . We recognise in this equation the scale-invariant integration measure; also a factor to account for the fact that a ball of volume ρ^4 can be placed in $1/\rho^4$ different ways in a unit volume; and finally a factor arising from the classical instanton action, $S_I = 8\pi^2/g^2(\rho)$.

Note that at this point we have departed from the classical calculation: perturbative fluctuations around the instanton break scale-invariance, promoting the bare g^2 to a running $g^2(\rho)$ in the usual way. This is crucial. When we insert the asymptotically free form of the coupling, we obtain

$$D(\rho) \propto \left(\frac{\rho}{\xi}\right)^6. \quad (6)$$

where ξ is the physical length scale of the theory. (The corresponding power in SU(2) would be $\rho^{7/3}$.) We observe that the number of instantons vanishes rapidly as $\rho \rightarrow 0$ (rather than diverging as it did in the classical theory). This makes it plausible that the introduction of a lattice will not affect the physics once $a \ll \xi$.

The behaviour of $D(\rho)$ in eqn(6) is only valid for $\rho \ll \xi$ since only then is $g^2(\rho)$ small enough for perturbation theory to be applicable. For $\rho \geq \xi$ the instantons will presumably overlap and the density is not calculable analytically. One of the things we want to learn from lattice calculations is what actually happens at larger ρ . Note that the characterisation of the topological charge density in terms of charges of size ρ might not be possible, even to a first approximation, in the real vacuum. Although we shall use that language for convenience in our discussions, we shall make some attempt to question its validity.

2.2 topology of lattice fields and cooling

A lattice gauge field consists of group elements, $U_\mu(x)$, on the links of the lattice. A lattice ‘instanton’ can be constructed straightforwardly by defining

$$U_\mu^I(x) = \mathcal{P} \exp \int_x^{x+a\hat{\mu}} A_\mu^I(x) dx \quad (7)$$

where the gauge potential $A_\mu^I(x)$ is as in eqn(3), but with its origin translated to the centre of a hypercube. (On a compact space, e.g. a hypertorus, we need to go to singular gauge, using the translated version of $g(x)$ in eqn(4), before imposing the periodic boundary conditions.) As long as $\rho \gg a$ any reasonable definition of topological charge will assign $Q = 1$ to this lattice field. If we are in a finite periodic volume of length La , then this $Q = 1$ lattice field will be close to being a minimum action configuration as long as $a \ll \rho \ll La$. (Exactly how close will depend on the particular lattice action being used.) If we now smoothly decrease ρ to values $\rho \ll a$ this lattice field will become indistinguishable from a gauge singularity and hence will have $Q = 0$. Thus we explicitly see the ambiguity in assigning a topological charge to a lattice gauge field.

Note that this ambiguity disappears as $a \rightarrow 0$. Indeed suppose a lattice field configuration is to be smoothly deformed from $Q = 1$ to $Q = 0$. This requires a topological fluctuation to be squeezed out of the lattice, as described above. While we do not know much about the structure of the original fluctuation (it will typically be on a size scale $\sim \xi$ which is beyond the reach of our analytic techniques) we do know that if the lattice spacing is sufficiently small then to reach $\rho \sim a$ the ‘instanton’ will have to pass through sizes $\xi \gg \rho \gg a$. In this region the density is calculable as we saw above, with a probability that is very strongly suppressed; at least as $\sim (\rho/\xi)^6$ for SU(3). So the changing of Q is conditional upon the involvement of field configurations whose probability $\rightarrow 0$ as $a \rightarrow 0$. Thus, as we approach the continuum limit this lattice ambiguity vanishes very rapidly. (And much more rapidly in SU(3) than in SU(2).) That is to say, the situation is much as with the calculation of any other physical quantity: one can only trust one’s results after performing the appropriate scaling analysis.

Since we are interested in learning about the sizes of the topological charges we need a lattice version of the continuum charge density $Q(x)$ defined in eqn(2). Let $U_{\mu\nu}(x)$ be the ordered product of link matrices around the plaquette labelled by the site x and the plane $\{\mu, \nu\}$. (For brevity we will refer to this group element as a plaquette.) As is well known, we can expand $U_{\mu\nu}(x) = 1 + a^2 F_{\mu\nu}(x) + \dots$ and so we can define a lattice topological charge $Q_L(x)$ as follows [21]:

$$Q_L(x) \equiv \frac{1}{32\pi^2} \epsilon_{\mu\nu\rho\sigma} \text{Tr} \{U_{\mu\nu}(x) U_{\rho\sigma}(x)\} = a^4 Q(x) + O(a^6). \quad (8)$$

(In fact we employ the version of this that is symmetrised with respect to forward and backward directions, so that the operator changes sign under reflection in any axis.) If we apply this formula to a smooth gauge field then we find, as expected, that the corrections are $O(a^2)$; for example, in the case of our instanton $Q_L = \int Q_L(x) dx = 1 + O(a^2/\rho^2)$.

If we apply $Q_L(x)$ to the real vacuum, however, we immediately encounter problems. The operator is dimensionless and so $O(a^6)$ actually means terms like $\sim a^6 F^3$, $\sim a^6 F D^2 F$ etc. For smooth fields these are indeed $O(a^6)$. However realistic fields (those that contribute to the path integral) have fluctuations all the way up to frequencies of $O(1/a)$. The contribution of these high frequency modes to the $O(a^6)$ terms will be $\delta Q_L(x) \sim a^6 \times 1/a^6 \sim O(a^0)$ (up to some powers of β that can be calculated in perturbation theory). Thus in the real world $Q_L(x)$ possesses interesting topological contributions that are of order $a^4 \propto e^{-\frac{16\pi^2}{33}\beta}$ (using the running coupling on scale a for g^2) and uninteresting ultraviolet contributions that are of order $1/\beta^n$. So as we approach the continuum limit, $\beta \rightarrow \infty$, the ultraviolet fluctuations dominate and completely mask the interesting physics.

Actually things are somewhat worse than this. Like other composite lattice operators, $Q_L(x)$ possesses a multiplicative lattice renormalisation factor: $\bar{Q}_L = Z_Q Q$ where $Z_Q \simeq 1 - 5.451/\beta + O(1/\beta^2)$ [12]. This looks innocuous, and indeed in the continuum limit it obviously is. However in the range of values of β where current lattice calculations are performed, typically $\beta \sim 6$, we see that $Z_Q \ll 1$, rendering the topological charge virtually invisible.

To deal with these problems we shall use the technique of ‘cooling’ [22] the fields. The idea rests on the observation that the problems are all caused by the ultraviolet fluctuations on wavelengths $\sim a$. By contrast, if we are close to the continuum limit, the topology is on wavelengths $\rho \gg a$. One can therefore imagine taking the lattice fields and locally smoothing them over distances $\gg a$ but $\ll \rho$. Such a smoothing would erase the unwanted ultraviolet fluctuations while not significantly disturbing the physical topological charge fluctuations. One could then apply the operator $Q_L(x)$ to these ‘cooled’ fields to reveal the topological charge distribution of the vacuum.

How do we cool a lattice gauge field? The simplest procedure is to take the field and generate from it a new field by the standard Monte Carlo heat bath algorithm subject to one important modification: we always choose the new link matrix to locally minimise the plaquette action. Since $Tr U_{\mu\nu}(x)$ measures the variations of the link matrices over a distance a , minimising the plaquette action is a very efficient way to erase the ultraviolet fluctuations. Obviously there are many possible variations on this theme and we shall return to that question shortly.

Thus the idea is that we take our ensemble of N gauge fields, $\{U^{I=1,\dots,N}\}$, perform a suitable number of cooling sweeps on each one of these, and so obtain a corresponding ensemble $\{U_c^{I=1,\dots,N}\}$ of cooled fields. We then extract the desired topological properties from these cooled fields. What are the ambiguities? As we cool, topological charges of opposite sign will gradually annihilate. This changes the topological charge density but not the total value of Q . Eventually this leads to a dilute gas of instantons. As we cool even further these isolated instantons will gradually shrink. Eventually they shrink within a hypercube and at this point even Q will change. (This will occur if we cool with a plaquette action on a large enough volume: other actions may lead to other outcomes.) Of course when an instanton becomes narrow it has a very peaked charge density and is impossible to miss. So we will certainly know when it disappears out of the lattice and can, if we think it appropriate, correct for that. So cooling provides a reliable method for calculating the total topological charge of a lattice

field. However the topological charge density changes continuously throughout the cooling process and so what we learn from it is far more ambiguous. For this reason we shall try to use as few cooling sweeps as possible and, in addition, we shall repeat the calculations for various numbers of cooling sweeps so as to try and disentangle any artifacts of the cooling procedure.

2.3 under-relaxed cooling

Consider first the case of SU(2) and suppose we are using a plaquette action. The part of the action that involves the link matrix $U_\mu(x)$ is proportional to $Tr\{U_\mu(x)\hat{\Sigma}(x;\mu)\}$ where $\hat{\Sigma}(x;\mu)$ is an SU(2) matrix proportional to the sum of the ‘staples’ around the link under consideration. So if we were choosing a new link matrix $U'_\mu(x)$ to locally minimise the action, we would choose $U'_\mu(x) = \hat{\Sigma}^\dagger(x;\mu)$. Repeating this procedure for all the links of the lattice would constitute the simplest type of cooling sweep. We might however imagine generalising it to the choice

$$U'_\mu(x) = c(\alpha U_\mu(x) + \hat{\Sigma}^\dagger(x;\mu)) \quad (9)$$

where c is a normalisation constant ensuring that the link matrix is unitary and α is a free parameter. (This has been called ‘under-relaxed’ cooling [13].) This will smoothen the fields for $\alpha \geq 0$. We will use this freedom to try and choose a form of cooling that is optimal for our purposes.

To use this method in SU(3), we simply apply it to the SU(2) subgroups that arise in the standard Cabibbo-Marinari algorithm.

We shall use three criteria for deciding what is the optimal choice of α .

- We want to use as few cooling sweeps as possible.
- We want to disturb the topological charge density as little as possible.
- We do not want instantons which initially have $\rho \sim a$ to broaden as we cool.

So the first thing we wish to do is to compare the different kinds of cooling sweeps. We calibrate them as follows. Discretise an instanton of size $\rho = 2a$ as in eqn(7). Now cool it until it disappears. Our criterion for disappearance is that the action drops below 10% of the continuum instanton action. We find that the number of cools, n_c , to do this varies with α approximately as follows:

$$n_c(\alpha) = 23 + 32\alpha. \quad (10)$$

(One can easily show that, at large α , n_c must increase linearly.) This is a measure of how effectively the different kinds of cooling erase high-frequency modes: and as expected we need more sweeps as we increase α .

Let us now ask how rapidly the topological structure changes under cooling. To address this question we construct classical instanton anti-instanton pairs of various widths and various distances apart. We then cool them and see how many sweeps it takes to annihilate them. We express the number of sweeps in units of the corresponding calibrated sweeps, i.e. in units of $n_c(\alpha)$ in eqn(10). An example is shown in Fig.1. In this plot we show how the action of an instanton anti-instanton pair, with $\rho = 3a$ and separation $9a$, varies with the number of cooling sweeps. We show separately what happens for $\alpha = 0$ and $\alpha = 2$. We observe that in

units of the calibrated sweeps, cooling with $\alpha = 2$ alters the topological structure more slowly than $\alpha = 0$ cooling. This is not a large effect but is characteristic of what we see with other examples.

In addition to the above studies we have also compared the effects of the different kind of cooling on thermalised field configurations. To be specific, on five $16^3 48$ lattice fields generated at $\beta = 6.0$. We cooled these with $\alpha = 0.0, 0.5, 1.0, 1.5, 2.0, 2.5$, and 3.0 . In Fig.2 we show how the action decreases with the number of (calibrated) sweeps. We see that the curves corresponding to $\alpha = 0$ and $\alpha = 2$ almost fall on top of each other. This confirms the fact that to a good approximation a calibrated sweep has the same effect on the ultraviolet lattice modes for any α .

As an aside we note that the action drops much further in the first $\alpha = 0$ cooling sweep than in the first $\alpha = 2$ (uncalibrated) sweep. To the extent that there is a worry about what might be happening at this early stage, there might be some advantage in the smoother under-relaxed cooling procedure.

Finally we note that while the value of Q_L after one calibrated cooling sweep is independent of α on three of the five configurations, it differed by 1 on two of them. To be precise, the fields cooled with $\alpha \geq 0.5$ all agreed with each other and the disagreement was with the $\alpha = 0$ case. It could be readily traced to a single ‘instanton’ that was narrow during the first few cooling sweeps, and which rapidly shrank out of the lattice with further $\alpha \geq 0.5$ cooling, but which broadened under $\alpha = 0$ cooling. This anomalous broadening must be a result of the non-trivial environment in which the narrow instanton is sitting. It is however something we would wish to suppress as much as possible and this is an argument for not using $\alpha = 0$.

We have seen that in appropriate units we can disturb the topological charge density less by using $\alpha \neq 0$ and that we simultaneously reduce the probability of $\rho \sim a$ artifacts surviving the cooling. Our studies are far from definitive and because of their low statistics might even be misleading; but they do serve to illustrate the criteria that it would make sense to use. Motivated by what we have found we shall use under-relaxed cooling with $\alpha = 1$ for the remainder of this paper.

3 Pattern recognition

Since the cooling algorithm is local it will erase the highest frequency modes first. Ideally we would like to stop the cooling once it has erased all the modes on scales $\lambda \ll \xi$ but before it has significantly affected the physically interesting modes on scales $\lambda \sim O(\xi)$. Such a clean separation is not possible in practice and by the time we have cooled enough to reveal the long-distance structure of $Q(x)$ we have certainly deformed that structure. Thus one has to perform the calculations for various numbers of cooling sweeps and attempt to identify those features that are relatively robust.

Because our cooling algorithm gradually deforms a field configuration towards the minimum of the action, the topological charge density will increasingly resemble a set of overlapping instantons and anti-instantons. As we cool further, those that are strongly overlapping will annihilate and the vacuum will become less densely packed. So in order to identify the

structure of $Q(x)$ we shall assume that it is given by an overlapping set of (anti)instantons of various sizes. This is of course a crude approximation. It also raises a fundamental question: how much of this structure is driven by the cooling and how much of it is intrinsic to the original uncooled field configuration? One way to try and answer this question is to increase β so that the separation between the physical and ultraviolet modes becomes better defined. We have therefore included calculations up to $\beta = 6.4$.

In this section we describe how we extract and categorise the topological structure of the cooled field configurations.

The first step is to use the peaks of $Q(x)$ to locate the centres of the topological charges and to provide a first estimate of their sizes. We then need to correct for the influence of the charges on each other. The next step is designed to reduce the number of false identifications. These may arise, for example, from secondary ripples on very large instantons. We implement two filters for this purpose. That there are in fact many mis-identifications is easy to show. We have n_I candidate instantons and $n_{\bar{I}}$ candidate anti-instantons. The total topological charge is therefore predicted to be $n_I - n_{\bar{I}}$. At the same time we can calculate Q directly from $\int Q_L(x)d^4x$. The quantity

$$\delta_Q \equiv |Q - (n_I - n_{\bar{I}})| \tag{11}$$

provides a direct measure of the mis-identification, and typically turns out to be substantial. At the same time this provides us with a criterion for choosing the parameters in our filters: they are chosen so as to minimise the value of $\langle \delta_Q \rangle$.

Our discussion so far has been based upon the topological charge density. Clearly there is information carried by the action density as well and one might ask whether it would be useful to incorporate that. We investigate this question in the last subsection and find that the action density has little new to tell us about the smaller charges that are easy to identify anyway, and is not able to resolve the larger charges where all the uncertainties lie. Thus for the remainder of the paper our analysis will be entirely based upon the topological charge density.

3.1 peaks and neighbours

Once we have cooled a field configuration we calculate the topological charge density using eqn(8). The peaks in this density are candidate locations of instantons. However it is our experience in dealing with smooth discretised instantons that it is dangerous to define a peak only with respect to the sites that are $\pm a$ away in any one direction. One instanton can readily produce peaks on sites across diagonals of a hypercube.

We therefore define $Q_L(x)$ to have a peak at x_0 if its value at $x = x_0$ is greater than at all the 3^4 sites belonging to the corresponding hyperbox centered on x_0 . (With an obvious modification to account for negative maxima.) Of course if two instantons happen to be close enough together, then we will miss one of them by using this criterion. However the probability of this occurring will decrease rapidly as a decreases. So, once again, as long as we perform a scaling analysis there is no ambiguity.

At this stage we have candidate positive charges at $\{x_i^+; i = 1, \dots, n_+\}$ and candidate

negative charges at $\{x_i^-; i = 1, \dots, n_-\}$. We shall make the customary assumption that only charges are with $Q = \pm 1$ are present. (It is non-trivial matter to test this assumption and we do not attempt to do so in this paper.) To obtain a first estimate of the sizes of these charges we can use the classical instanton relation between the topological charge density at the peak and the width:

$$Q_p = \frac{6}{\pi^2 \rho^4}. \quad (12)$$

This relation is for a continuum instanton. It applies equally well for a large lattice instanton, but will become inaccurate for smaller instantons where $O(\frac{a^2}{\rho^2})$ lattice corrections become significant. In practice we use a lattice corrected version of eqn(12) as described in the Appendix.

We now have a first estimate for the positions, x_i^\pm , and sizes, ρ_i^\pm , of the (anti)instantons. However we know that the value of $Q_L(x)$ at $x = x_i^\pm$ will receive contributions from the tails of all the other (anti)instantons and so may not be an accurate reflection of the peak value of the topological charge that is centered there. To correct for this we have implemented the following iterative procedure.

We shall make two main approximations. First we shall assume that the topological charge is additive. Secondly we shall only attempt to calculate the corrections to the sizes, ρ_i^\pm , and not to the locations, x_i^\pm . These are approximations that should be improved upon. Under these assumptions we can write

$$Q(x_i^\pm) = Q_p(\rho_i^\pm) + \sum_{x_j^\pm \neq x_i^\pm} Q_I(|x_j^\pm - x_i^\pm|; \rho_j^\pm) \quad (13)$$

where $Q_p(\rho)$ is the peak value of a topological charge of radius ρ (as given in eqn(12) and with the lattice corrections as in the Appendix) and $Q_I(|x - x_0|; \rho)$ is the contribution to the charge density at x from an instanton of size ρ located at x_0 . We use the continuum expression for this

$$Q_I(|x - x_0|; \rho) = \frac{6}{\pi^2} \frac{\rho^4}{(x^2 + \rho^2)^4} \quad (14)$$

with the opposite sign for anti-instantons. While one should improve upon this expression by including lattice corrections at small- ρ , this is not necessary to a first approximation, because the corrections to ρ that are embodied in eqn(14) turn out to be modest. Note that to avoid cluttering the equations we have dropped the subscript on Q_L .

What we know in eqn(13) are the values of the $Q(x_i^\pm)$ and what we want to solve for are the ρ_i^\pm . One can attempt to do this by iteration, using eqn(12) and $Q_p(\rho_i^\pm) = Q(x_i^\pm)$ to provide us with our starting values of ρ_i^\pm . We pick say the charge at x_1^+ and calculate the contribution of all the other peaks using eqns(13,14). From the renormalised peak value we extract a corrected value of ρ_1^+ to replace our first guess. We go to the next charge and repeat the same procedure there except that we use the updated value of ρ_1^+ in calculating Q_I . Repeating this procedure at each relevant site constitutes one iteration. We perform as many iterations as are required to reach convergence. Our criterion for convergence is that the change in ρ during the final iteration should satisfy $\delta\rho \leq 0.001\rho$ for all the charges.

In practice we have applied the above procedure with a slight modification: if at any stage the apparent sign of a charge changes when we take into account the influence of the other charges, then this charge is removed and plays no further part in the analysis. The reason for doing this is that given the approximate nature of the correction, if it makes such a large difference then we cannot be confident that there is in fact a charge at that location. To throw the charge away is of course an arbitrary choice. Fortunately this arises very infrequently. For example on 20 $16^3 48$ lattices after 23 cooling sweeps one peak was removed from 6 configurations and four peaks from one configuration; despite the fact that the average configuration contained 169 peaks. In this sense the modification is indeed slight.

We remark that the above procedure has always converged; presumably because our starting point is always close enough to the final solution. We have explicitly checked that the final solution does not depend on the order in which the peaks are considered, and, more to the point, that neither do the peaks that are thrown out because they change sign.

How much of a difference does it make to estimate the instanton sizes using eqn(13) rather than just applying eqn(12) to the observed peak heights? In Fig.3 we show what happens on a test sample of 20 $\beta = 6.0$ $16^3 48$ field configurations after 23 cooling sweeps. On the x-axis we plot the quantity

$$\frac{\delta\rho}{\rho} = \left| \frac{\rho_{final} - \rho_{orig}}{\rho_{orig}} \right| \quad (15)$$

where ρ_{orig} is the initial estimate of the size using eqn(12), and ρ_{final} is the value obtained after solving eqn(13). On the y-axis we plot the average number of times a value of $\frac{\delta\rho}{\rho}$ occurs per field configuration. We observe that the fractional change in ρ is typically at the $\sim 5\%$ level; that is to say, small but significant.

We note from eqn(13) that subtracting a small constant δQ from the peak value of $Q(x)$, leads to a fractional change in the width $\delta\rho/\rho \propto \rho^4 \delta Q$. We would therefore expect that charges with small ρ would be practically unaffected by the corrections in eqn(13), but that the fractional change would rapidly increase with ρ and, at some point, would cease to be reliable. In Fig.4 we show how the average value of the fractional change in ρ depends on the final value of ρ , in our test sample of configurations. We see that $\langle \delta\rho/\rho \rangle$ is very small up to $\rho \sim 5$, which, as we shall shortly see, is roughly where the charge density, $D(\rho)$, has its maximum at $\beta = 6.0$. It then grows rapidly with ρ but remains small enough to be credible up to $\rho \sim 10$. Thereafter it becomes large and our approximations are presumably inadequate. However, as we shall see, there are almost no instantons for $\rho \geq 10$ and so we believe that our procedure provides a reasonable first approximation for the range of ρ relevant to our calculations.

3.2 filtering the peaks

At this stage we have a set of candidate charges. We claim to know their positions and their widths. If this was all that was needed then we would expect that the value of δ_Q in eqn(11) would be zero. We show in Table 1 what the average values of this quantity actually are for the $24^3 48$ configurations at $\beta = 6.2$. We also show, for comparison, the value of $\sqrt{\langle Q^2 \rangle}$ and

the average number of charges, $\langle N_{tot} \rangle \equiv \langle n_I + n_{\bar{I}} \rangle$. We do this for various numbers of cooling sweeps.

We observe that there is a substantial mismatch between the value of Q as calculated directly and that obtained from the peaks of $Q(x)$. The former is certainly reliable (up to errors in the lattice corrections, which are negligible relative to δ_Q). So either some charges do not show up as peaks, and so we have missed them, or some of the peaks in $Q(x)$ are not topological charges. We cannot deal with the first possibility without a much more sophisticated correction procedure than that embodied in eqn(13). This is beyond the scope of the present paper. To address the second possibility we shall calculate some further properties of the topological charge density around the peaks and use these to “filter out” the peaks that are most likely not to be instantons.

3.2.1 a width filter

For an instanton of size ρ the charge within a radius R is given by

$$Q(|x| \leq R) = 1 - 3 \left(\frac{1}{1 + \frac{R^2}{\rho^2}} \right)^2 + 2 \left(\frac{1}{1 + \frac{R^2}{\rho^2}} \right)^3 \quad (16)$$

(This will require significant lattice corrections for small ρ , as discussed in the Appendix.)

We can use eqn(16) to calculate ρ from $Q(|x| \leq R)$. For an isolated classical instanton we will get the same value of ρ whatever value of R we choose. In an environment where instantons overlap this will not be the case. If we correct for this overlap by using an obvious generalisation of eqn(13) then the extracted ρ should become independent of R .

Our filter is therefore as follows. As described earlier, for each peak in $Q(x)$ we calculate a value of the width, ρ , using the (corrected) value of $Q(x)$ at the peak. We then choose some value of R and calculate the corresponding widths ρ_R from the (corrected) values of $Q(|x| \leq R)$, as described above. If the peak represents a real instanton then we expect that the values ρ and ρ_R should be similar. We therefore impose the condition

$$\text{Max} \left(\frac{\rho_R}{\rho}, \frac{\rho}{\rho_R} \right) - 1 < \epsilon_R \quad (17)$$

where ϵ_R is a small number that will be fixed by minimising the quantity δ_Q in eqn(11). Only if a peak satisfies this condition will it be counted as a genuine topological charge. In practice we shall use $R = 2$ in our later calculations. (Note that we shall switch between physical and lattice units as convenient, when there is no ambiguity.)

3.2.2 a distance filter

Very broad instantons are likely to be significantly distorted and so one needs a reasonably generous value of ϵ_R in eqn(17) if one is not to run the risk of filtering out too many genuine topological charges. It is therefore useful to supplement the previous filter with an additional one.

We choose to focus on the possibility that a very broad instanton might possess a long-wavelength ripple across its surface which then leads to a misidentification of the structure as containing two (or more) broad instantons. (This is a possibility because the small number of cooling sweeps that we shall be using will not affect long-wavelength modes.)

Our filter consists of the following steps.

1. Consider a randomly chosen peak of $Q(x)$ at position x_0 with width ρ_0 .
2. Identify the peak nearest to it. If this has the opposite sign accept the original peak. If it has the same sign, follow the steps below.
3. Let ρ_n, x_n be the width and position of the nearest neighbour. Let ρ_c be a cut-off value to be chosen. Then we accept the original peak if either it or the nearest neighbour is narrower than ρ_c i.e. if $\rho_0 \leq \rho_c$ or $\rho_n \leq \rho_c$.
4. If both peaks are broader than ρ_c and if the distance between them is small compared to their sizes then we reject the peak under consideration. The detailed criterion is $|x_0 - x_n| \leq \epsilon_c(\rho_0 + \rho_n)$ where ϵ_c is a small number to be chosen.

We consider each peak on the lattice in this way. The peaks are considered in a random order and therefore the choice of which of two broad nearby peaks gets thrown out is in reality random.

3.2.3 using the filters

In practice we apply the distance filter first and apply the width filter to those peaks that survive. We have the parameters ϵ_R, ρ_c and ϵ_c to fix. This is done by minimising δ_Q , in eqn(11), with respect to variations in all three parameters simultaneously. This is a time-consuming calculation and we typically perform it on a subset of ~ 20 of the configurations, and then use the parameters so determined to analyse the whole ensemble.

The quantity δ_Q will often have several minima that are not significantly higher than the absolute minimum. In such situations we choose the minimum that leads to fewer peaks being rejected. This is to avoid loose cuts that lead to the loss of too many real instantons along with the false peaks. In Table 2 we list the filter values we use in the calculations of this paper.

We now give an example of the application of the above filters, using our $24^3 48$ lattice fields at $\beta = 6.2$. We consider the three ensembles obtained after 23,32 and 46 cooling sweeps. In Table 2 we see the filter parameters and the corresponding values of δ_Q . We observe that δ_Q is dramatically reduced when compared to the unfiltered values in Table 1. The width filter used here involved $R = 2$. The corresponding values with $R = 3$ are shown in Table 3. The results are not dissimilar.

In order to achieve these acceptably small mismatches between Q and $n_I - n_{\bar{I}}$, how severely do we need to change the distribution of charges? Not very much is the answer. In Table 4 we show the number of peaks before and after the filters are applied. Even for the smallest number of cooling sweeps, we only lose $\sim 10\%$ of the peaks. In Fig.5 we show the number of instantons per configuration as a function of the size ρ , before and after applying the filters. Here we see that the change is concentrated amongst the very largest instantons. This is as it

should be: it is these charges, with their very small charge densities and their large overlaps with many other charges, that are the hardest to extract reliably.

Although the purpose of our filters is to reject false peaks, it is inevitable that occasionally they will reject real charges. This is especially so with the distance filter: two broad instantons may be close together just by chance. It would be useful to have some crude estimate of this. One could do this by throwing the charges into our space-time box, with the observed size density, and seeing how often they would be rejected by the distance filter. In throwing the charges into the box, one should incorporate some broad features of the correlations. As we shall see one such feature is that the nearest neighbour tends to be of the opposite sign; and a second is that there is a strong suppression of (anti)instantons very close to each other. We have not implemented such a realistic model, but have simply thrown the instantons into the box entirely at random. In that case we find that the number of real rejected instantons is close to the actual number we reject. It should be clear that the qualitative effect of modifying the random distribution to include the features we just described, will be to markedly reduce the number of mistaken rejections. Thus we anticipate that only a small fraction of the charges rejected are real ones. However this is only a qualitative argument and it is certainly no substitute for an explicit and careful “background” calculation: this still needs to be done.

We have seen that by the addition of two physically motivated filters we are able to reduce the discrepancy, δ_Q , quite dramatically and that this only involves the rejection of a small percentage of the peaks. Moreover the rejected peaks are concentrated amongst the very broadest charges, as they should be. In the remainder of our work these are the filters that we shall employ.

3.3 the action density

Before moving onto our results, we briefly ask whether there is much to be gained by using the action density, $S(x)$, in addition to or in place of the topological charge density.

What do we expect? Generally $S(x) \geq |Q(x)|$, if we use a normalisation where $S(x) = |Q(x)|$ for a self-dual field. As we cool we shall eventually be driven to such a self-dual solution (up to lattice corrections). It is only when $S(x) \simeq |Q(x)|$ that one can use analogues of eqn(13) for the action so as to estimate widths from the action densities. In Fig.6 we show how the ratio $\sum S(x)/\sum |Q(x)|$ varies with the number of cooling sweeps. (This comes from 5 16³48 configurations at $\beta = 6.0$.) We see that the fields are far from being self-dual.

If we ignore the non-self dual nature of the fields and extract widths from the peaks in the action density, then we obtain the size distributions shown in Fig.7 and Fig.8. We also show, for comparison, the corresponding distributions that we obtain from the topological charge density. (Note that both analyses simply use the peak height, with no added filters of the kind described above.) We observe that for small ρ the distributions are essentially identical while at large ρ the distribution from the action is suppressed, and that this effect is stronger for fewer cools.

This can be qualitatively understood in the approximation where we think of the extra non-selfdual action, $\delta S = \sum S(x) - \sum |Q(x)|$, as being smoothly distributed over the whole volume. If we calculate ρ from the peak action density, then this increment will shift instanton

sizes to smaller values. Narrow instantons have large peaks that will be little changed by this addition. On the other hand the action density will never be smaller than $S(x) = \delta S/volume$ and this provides an upper limit on the ρ that one extracts. This effect should be weaker for a larger number of cooling sweeps because $\delta S/volume$ decreases – see Fig.6. This certainly provides a first approximation to what we observe in Fig.7 and Fig.8. At small ρ no change; at large ρ a quite sharp cut-off; at medium ρ an enhancement in the size density from the action as one would expect if larger peaks had been shifted to smaller ones. The numbers roughly fit too, except it is clear that only a small fraction of the broad charges have been shifted to smaller values: most of them have apparently disappeared. This is to be expected. If we have a very broad instanton overlapping with a very broad anti-instanton we can see two peaks in $Q(x)$ because of the sign difference. $S(x)$ however is always positive and is quite likely not to show two peaks - just a single broad peak covering the pair.

One can go a step further and ask whether the peaks in $S(x)$ are in fact associated with peaks in $Q(x)$. In Table 5 we show the number of peaks obtained from $S(x)$ and $Q(x)$ for 23 and 46 cooling sweeps. We also show how many of the peaks in $S(x)$ are associated with peaks in $Q(x)$: either because they are at the same site or because they are within 2 lattice spacings. We observe that the latter accounts for nearly all the action peaks.

We conclude that as long as we work with a small number of cooling sweeps the action density loses most of the information about the larger topological charges, although it does reproduce the narrower topological charges that we find using $Q(x)$. Thus we shall ignore the action in the remainder of this paper in the expectation that including it would yield marginal benefits.

4 Size distribution of instantons

The size distribution of the topological charges, $D(\rho)$, is the simplest quantity characterising the vacuum topological structure. In this section we shall explore it in some detail.

4.1 general features

In Fig.9 we show the size distribution as obtained on the 16^348 lattice fields at $\beta = 6.0$ for various number of cooling sweeps, n_c . The quantity plotted is the average number of charges, $N(\rho)$, in each bin, $\Delta\rho$ of ρ . Thus $N(\rho) \simeq VD(\rho)\Delta\rho$, where V is the space-time volume.

We see that there is a rapid decrease in the total number of charges as we cool the fields. This is presumably the result of nearby charges of opposite sign annihilating. Other features, such as the location of the maximum of the distribution, appear to vary much more weakly which suggests that they are robust features of the fields prior to cooling.

It will be useful to choose a few quantities by which we can characterise the size distributions. An obvious measure is the average value of the size, $\bar{\rho}$. Since the distributions are not grossly asymmetric, this will nearly coincide with the maximum. Another quantity we can use is the half-width, σ_ρ , of the distribution. Finally there is the total number of charges, \bar{N}_{tot} . In Table 6 we list the values of these quantities for all our values of β and n_c .

When discussing the scaling properties of these various quantities we will need to know how the lattice spacing varies over our range of β . For this we need some physical quantity expressed in lattice units. We choose the confining string tension, σ , because that has been calculated very accurately. The relevant values are [23],

$$a\sqrt{\sigma} = \begin{cases} 0.2187(12) & \beta = 6.0 \\ 0.1608(10) & \beta = 6.2 \\ 0.1216(11) & \beta = 6.4. \end{cases} \quad (18)$$

Wherever we discuss lengths or volumes in physical units, it will be by using eqn(18) to set the scale.

Occasionally it will be useful (or illuminating) to express things in MeV units. There are, of course, all kinds of ambiguities in introducing MeV units into a theory which, unlike QCD, does not describe the real world. This is discussed in [20] where an analysis of the hadron spectrum in the quenched approximation is found to lead to an estimate

$$\sqrt{\sigma} = 440 \pm 15 \pm 35 MeV. \quad (19)$$

Here the first error is statistical and the second is a systematic error that reflects in part the fact that Quenched QCD does not in fact represent the real world. Wherever we present quantities in MeV or fm units it will be through using eqn(19).

Before moving to a detailed consideration of the size distribution there is at least one qualitative conclusion we can immediately draw. We see from Fig.9 and eqn(18) that $\bar{\rho} \sim 5a \sim 1/\sqrt{\sigma} \sim 0.5 fm$. Thus the typical instanton size is quite large. Given that the average charge has a diameter of $2\bar{\rho} \simeq 10a$. and that there are about 180 charges at 23 cools, it is clear that the $16^3 48$ lattice must be densely packed. This is so even after 46 cools. Thus our first qualitative conclusion is that instantons are large and strongly overlapping. This is a different picture to the one that apparently underlies typical instanton liquid model calculations [4].

4.2 packing fraction

As we have just seen, our instanton gas is dense. Since the largest instantons are more difficult to identify unambiguously, it is interesting to ask if the gas is dense even if we exclude such instantons.

To address this question we define a packing fraction $f(\rho)$ by

$$f(\rho) = \frac{1}{V} \int_0^\rho n(\rho) v_I(\rho) d\rho \quad (20)$$

Here $n(\rho)$ is the number of instantons of size ρ , $v_I(\rho)$ is the space-time volume occupied by an instanton of this size and V is the total space-time volume. That is to say, $f(\rho)$ is the fraction of space-time occupied by instantons of size $\leq \rho$.

Since the instanton core is smooth, there is some ambiguity about defining $v_I(\rho)$. We shall choose to define it as a 4-sphere of radius ρ : a conservative choice. So $v_I(\rho) = \pi^2 \rho^4 / 2$.

Using our calculated size distributions, and this definition of the instanton volume, we can calculate $f(\rho)$. In Fig.10 we plot f against $\rho/\bar{\rho}$ as calculated at $\beta = 6.4$ after $n_c = 30, 50, 70$ and 80 cooling sweeps. We observe that $f(\rho = \bar{\rho}) \geq 1$: so even if we include only those instantons that are of below average size, the gas is still dense. Moreover, even though the average instanton size decreases as n_c decreases (see Table 6), the total number of charges increases sufficiently rapidly that the packing fraction itself gets larger. Thus it is difficult to avoid the conclusion that the ‘instanton gas’ in the real vacuum is a dense one, irrespective of any uncertainties concerning the identification of the larger instantons.

4.3 variation with volume

Given that our instantons are large, it is important to check if our size distribution is not distorted by finite volume effects. In Fig.11 we compare the size distributions as obtained on the $16^3 48$ lattices and on the very much larger $32^3 64$ lattices, both generated at $\beta = 6.0$ and both after 46 cooling sweeps. (The distribution on the larger lattice has been normalised to the volume of the smaller.) We observe that there are no statistically compelling differences between the two distributions. In particular, at very large ρ , where any differences should be most pronounced, the distributions are virtually identical. We conclude that our $16^3 48$ lattice at $\beta = 6.0$ suffers from no significant finite volume effects. Since the $24^3 48$ lattice at $\beta = 6.2$ and the $32^3 64$ lattice at $\beta = 6.4$ have approximately the same volume in physical units as this lattice, we shall assume that none of our distributions suffer significant finite volume corrections.

4.4 scaling with β

The next question, whether the size distribution scales as $a \rightarrow 0$, is less straightforward. The reason, seen in Fig.9, is that the number of charges varies rapidly with the number of cooling sweeps. However a cooling sweep is not a procedure that scales; 23 cooling sweeps at $\beta = 6.0$ are certainly not equivalent to 23 cools at $\beta = 6.2$ or 6.4. So at what level of cooling should we compare the size distributions at different values of β ?

Indeed we can start with a more basic question: is there any evidence that one can choose the number of cools so that the distributions scale? The answer to this question appears to be in the affirmative. In Fig.12 we show the size distributions after 23 cools at $\beta = 6.0$, 46 cools at $\beta = 6.2$ and 80 cools at $\beta = 6.4$. The densities have been scaled by the physical volume, and ρ is expressed in units of the string tension. So exact scaling would imply that for some choice of the number of cools the distributions should coincide. What we infer from Fig.12 is that an approximate coincidence does indeed appear to be possible.

To be more quantitative we need to set up an equivalence between the number of cooling sweeps at $\beta = 6.0, 6.2$ and 6.4. We do so as follows. If the distribution scales then so does the number density. Let the average number of charges per unit physical volume be $N(\beta; n_c)$, where n_c is the number of cooling sweeps and eqn(18) is used to define the unit physical volume. Then n_c cooling sweeps at β are defined to be equivalent to n'_c cools at β' if the

number densities are equal:

$$N(\beta; n_c) = N(\beta'; n'_c) \quad (21)$$

In Table 6 we show how the total number of charges, N_{tot} varies with β and n_c . The volume of an $L_s^3 L_t$ lattice is $V = \{L_s a \sqrt{\sigma}\}^3 L_t a \sqrt{\sigma}$ in physical units, and using the string tensions in eqn(18) we can calculate $N = N_{tot}/V$ in each case and that is also given in Table 6.

At each β we can interpolate between the values in Table 6, so as to obtain the number density as a function of n_c . These interpolations can then be used in eqn(21) to find equivalent sets of n_c at different values of β .

In fact we immediately see from Table 6 that

$$n_c = \begin{cases} 23 & \beta = 6.0 \\ 46 & \beta = 6.2 \\ 80 & \beta = 6.4. \end{cases} \quad (22)$$

are, within errors, equivalent at the indicated values of β . (This is no accident of course: the number of cooling sweeps was chosen after a preliminary study designed to produce such an equivalence.) We note the corresponding values of $\bar{\rho}$ and σ_ρ , form dimensionless ratios with $a\sqrt{\sigma}$, and plot these against $a^2\sigma$ in Fig.13. The reason for plotting things this way is that we expect the leading lattice corrections to such dimensionless ratios of physical quantities to be $O(a^2)$. (We assume that $\bar{\rho}$ and σ_ρ are physical quantities in this sense.) That is to say, for small enough a we can extrapolate to the continuum limit using

$$\bar{\rho}(a)\sqrt{\sigma}(a) = \bar{\rho}(0)\sqrt{\sigma}(0) + ca^2\sigma \quad (23)$$

with a similar expression for σ_ρ . These will be straight lines in Fig.13 and the best fits are shown there. As we can see eqn(23) is compatible with our data. From these fits we obtain the continuum predictions:

$$\bar{\rho} = 1.235(20)\frac{1}{\sqrt{\sigma}} \simeq 0.56(5)fm \quad (24)$$

and

$$\sigma_\rho = 0.242(16)\frac{1}{\sqrt{\sigma}} \simeq 0.11(1)fm \quad (25)$$

where we have used eqn(19) to introduce fermi units.

We note that we are not able to derive a continuum limit for other (equivalent) sets of cooling sweeps, because the largest number of cools at $\beta = 6.4$ corresponds, roughly, to the smallest number at $\beta = 6.0$.

As far as the density of charges is concerned, the continuum limit is trivially obtained, because eqn(21) ensures that the number density at an equivalent number of cooling sweeps will be independent of β . Since this density varies so rapidly with the number of cools, it is probably not useful to attempt any conclusion other than the qualitative one that the charges are densely packed.

4.5 variation with cooling

As we have seen, most quantities that we calculate vary to some extent with the number of cooling sweeps. Since we are interested in the physics of the uncooled vacuum, the logical procedure would be to try and take the $n_c \rightarrow 0$ limit of our calculated values. However, to do so would be to ignore the fact that our procedures become increasingly unreliable in that limit. For example, the way we correct the instanton peak height in eqn(13) involves assumptions that will break down as the instanton gas becomes increasingly dense, as it does when n_c decreases. Thus it might be that the observed decrease of, say, $\bar{\rho}$ as n_c decreases merely reflects this increasing unreliability.

In the face of this uncertainty, our approach is as follows. Where we wish to draw a qualitative conclusion, we check whether the effect becomes more pronounced as n_c decreases. If that is the case, we take it to be evidence that the effect under consideration is indeed a property of the uncooled vacuum. An example of this is our conclusion that the instanton gas is dense. If, on the other hand, we wish to make a statement that is quantitative, then we pick some small number of cooling sweeps at some β and then extrapolate to the continuum limit at an ‘equivalent’ $n_c(\beta)$ as described above. If the variation with n_c of the quantity under consideration is small enough to be compatible with the errors of our pattern recognition algorithm, then there is some reason to believe that our calculation is relevant to the uncooled vacuum. An example is our calculation above of the average instanton width.

To illustrate the uncertainties, we show in Table 7 how the properties of a *single* configuration, taken from our $\beta = 6.4$ ensemble, vary with the number of cooling sweeps, n_c . (Note that this configuration has not been subjected to any filtering procedure.) The total number of charges, N_{tot} , varies so rapidly with n_c that we cannot hazard any guess at all about the number in the uncooled vacuum. This is as it should be: perturbative fluctuations in $F\tilde{F}$ can always be interpreted as a suitable ensemble of strongly overlapping topological charges, rendering the question of the total number fundamentally ambiguous. The average width, $\bar{\rho}$, and typical fluctuations about this average, σ_ρ , vary much less and one might feel entitled to infer, for example, that the average width in the uncooled vacuum is $\bar{\rho} \sim 9 \pm 1$ in lattice units. The decrease in $\bar{\rho}$ as $n_c \downarrow$ is what one would naively expect: perturbative fluctuations will, on the average, increase the peak heights in $|Q(x)|$ and this will translate into smaller values of ρ via eqn(12). The ratio $\sigma_\rho/\bar{\rho}$ shows little variation with n_c and it seems safe to infer a value of $\sim 0.20 \pm 0.02$ for it. Finally, the total packing fraction f is always large and for small n_c increases with decreasing n_c , suggesting that it is safe to infer that the instanton gas is dense in the uncooled vacuum. (Note that the increase of f for large n_c is presumably an artifact of the lack of filtering – compare with Fig.10.)

4.6 small ρ and large ρ

In addition to the global features of $D(\rho)$, such as $\bar{\rho}$, the tails of the distributions are also of interest. We recall that at small ρ we have the prediction from eqns(5,6) that $N(\rho) \propto \rho^6$. This simple form neglects powers of $\log \rho$ (there are factors of $1/g^2(\rho)$ in $D(\rho)$ that arise from the symmetries and which are subsumed into the ‘...’ in eqn(5)) so that it is only at *very*

small ρ that we would expect it to hold. And, of course, at very small ρ the cooling will erase and alter the distribution. So although we shall fit

$$N(\rho) \propto \rho^{\gamma_s} \quad : \rho < \bar{\rho} \quad (26)$$

we are only looking for a trend: that as a and the fitted range are reduced, and the number of cooling sweeps becomes small, γ_s should approach the predicted value of $\gamma_s = 6$.

Because there are no analytic predictions at large values of ρ the behaviour there is of particular interest. We have tried both exponential and power like fits to the large- ρ tails of our distributions. In practice the latter have significantly better χ^2 and are therefore the ones we present here. That is to say we fit

$$N(\rho) \propto \frac{1}{\rho^{\gamma_l}} \quad : \rho > \bar{\rho} \quad (27)$$

for the power γ_l .

In Table 8 we present some power fits to the small- ρ tails of our various size distributions. We show the range fitted (in units of $1/\sqrt{\sigma}$). The χ^2 of the fit is generally reasonable; indeed this served as one criterion for which range of ρ to fit. We observe that while the value of γ_s does vary a great deal, there does appear to be a trend that as we go to smaller a and to a smaller number of cooling sweeps the value is closer to the asymptotic prediction of $\gamma_s = 6$.

In Table 9 we present similar fits to the large- ρ tails. The values seem quite consistent, suggesting a power that gradually decreases from $\gamma_l \sim 12$ to $\gamma_l \sim 10$ as we increase the number of cools over our range. We also find that there appears to be a trend for this power to increase if we shift our fitting range to larger ρ – but we cannot be certain of this with our statistical accuracy. In any case, it is clear that the suppression at large ρ is much more severe than the $D(\rho) \propto 1/\rho^5$ that one would obtain with a coupling that freezes to some constant value at large distances. This shows that the full non-perturbative vacuum imposes a sharp infrared cut-off on the sizes of instantons.

5 Correlations of the instantons

In this section we investigate the correlations between the topological charges in the vacuum. We shall begin with the simplest question: how close are nearest neighbour charges and how does this depend on their relative signs. This will confirm our picture of a densely packed vacuum, and so naturally leads to the question whether these charges show any aspects of a dilute gas. We shall see that the smallest charges do and the very large ones don't. However the medium-sized charges show an unexpected behaviour which leads us to investigate the charge correlations in much greater detail. We find long range charge correlations amongst the smaller charges and, separately, amongst the larger charges, which is related to an anti-correlation between the smaller and the larger charges. This effect weakens as we increase the number of cooling sweeps, so suggesting that it reflects a property of the uncooled fields.

5.1 (nearest) neighbours

We begin by calculating the number of charges that are a distance R from a given charge. We do so separately for the case where the charges have the same sign ('like') and where they have the opposite sign ('unlike'). These distributions are calculated by counting the number of (un)like charges in the spherical shell of width δR a distance R away from each charge. The distributions are then normalised by the volume of each shell (for the lattice under consideration and taking the periodicity into account). So at larger R , as the correlations die away, we would expect each of these two distributions to go to a constant value and that this value should be the same.

In Fig.14 we show the distributions we obtain after 23 cooling sweeps at $\beta = 6.2$. These have been normalised so that they go to unity at large R . There are three features one immediately notes. At small R there is a strong suppression. Just after that there is a strong enhancement of unlike charges and a slight enhancement of like charges. Finally at large R the distributions are constant as expected. (The slight enhancement of like charges at very small R is likely to be an artifact of our procedures.)

The suppression at short distances extends much too far to be related to the fact that our definition of a peak uses 3^4 hypercubes. In addition, it also occurs on the unfiltered data and so is not a product of our filtering procedure.

We note that the like distribution is suppressed to larger distances than the unlike one. That is to say, the nearest neighbour is more likely to be a charge of the opposite sign. This means that topological charges are 'screened' by neighbouring charges. This is reasonable: an $I\bar{I}$ pair will usually have a lower action than an II pair. Not so expected is the fact that $N_{unlike}(R)$ shows a slight dip just after the enhancement. This coincides with the enhancement in $N_{like}(R)$ as we see in Fig.14. It indicates that there is a region of R where we have 'anti-screening'. We shall return to a more detailed investigation of this potentially interesting phenomenon shortly.

The suppression at small R and the immediate subsequent enhancement are best analysed by focussing on the nearest neighbours to each charge. In Table 10 we list the average distances to the nearest charges of the same sign and of the opposite sign. These are presented in physical units using eqn(18). We note that these distances increase with the number of cooling sweeps. One might try to explain this by arguing that under cooling the nearest unlike charges should annihilate and disappear; while like charges should repel each other since that lowers the action. Of course this argument disregards the complicated nature of the actual environment around each charge.

If we look at an equivalent number of cooling sweeps, as given in eqn(22), we see that the distances look nearly independent of a . This reassures us that a is small enough that we can extrapolate to the continuum limit using only the leading $O(a^2)$ correction just as we did in eqn(23). Doing so we find that the distance to the nearest like and unlike charges is

$$\bar{R}_{like} = 1.081(15) \frac{1}{\sqrt{\sigma}} \sim 0.49 fm \quad (28)$$

and

$$\bar{R}_{unlike} = 0.993(13) \frac{1}{\sqrt{\sigma}} \sim 0.45 fm \quad (29)$$

where we have used eqn(19) to introduce fermi units.

From eqns(24,25) and eqns(28,29) we see that

$$\frac{\bar{\rho}}{\bar{R}} \sim 1.2 \quad (30)$$

and this confirms our previous conclusion that what we have is certainly not a dilute gas.

Although we see from Table 10 that there is some variation of \bar{R} with the number of cooling sweeps, we note a similar variation for $\bar{\rho}$ in Table 6. Thus eqn(30) is robust against cooling and is presumably also a property of the uncooled fields.

5.2 how dilute a gas?

The fact that $\bar{\rho}/\bar{R} \sim 1$ and that nearest neighbours are much more likely to be of the opposite sign, tells us that the topological charges do not form a dilute gas. It is probable however that the smaller charges are dilute; if they are weakly correlated to the large instantons, then they might still lead to some physics that one would associate with a dilute gas.

To investigate this possibility we note that in a dilute gas we have $\langle Q^2 \rangle = N_{tot}$, where N_{tot} is the total number of charges. Thus a measure of how close we are to a dilute gas is provided by seeing how close the quantity $\langle Q^2 \rangle / \langle N_{tot} \rangle$, or the quantity $\langle Q^2 / N_{tot} \rangle$, is to unity. Since we are interested in seeing whether the smaller instantons form such a dilute gas, we define the quantity

$$P(\rho_c) \equiv \left\langle \frac{Q^2(\rho \leq \rho_c)}{N_{tot}(\rho \leq \rho_c)} \right\rangle. \quad (31)$$

Here $Q(\rho \leq \rho_c) = n_I(\rho \leq \rho_c) - n_{\bar{I}}(\rho \leq \rho_c)$ is the total topological charge of those charges that have a size less than ρ_c ; and $N_{tot}(\rho \leq \rho_c)$ is the corresponding total number of charges. So how close P is to unity, provides a measure of how much these charges behave like a dilute gas.

In Fig.15 we show how $P(\rho_c)$ varies with ρ_c for the $\beta = 6.2$ ensemble after 23 cooling sweeps. We observe that if we include charges with widths up to $\rho \simeq 5$ the value of P remains close to unity indicating a dilute gas structure. As we increase ρ_c beyond this value, P begins to increase rapidly, becoming much larger than unity. Around $\rho_c \simeq \bar{\rho} \simeq 6$ the value of P begins to fall and continues falling to values $\ll 1$. The value for $\rho_c \rightarrow \infty$ is the value one gets for P when one includes all the charges.

The way P behaves at small and at large ρ_c is not too surprising. For sufficiently small instantons the combination of low density and small sizes would make them behave like a dilute gas. For large overlapping instantons, on the other hand, we would expect a dominance of pairs of opposite sign which would suppress the fluctuations of $Q = n_I - n_{\bar{I}}$ for a given value of $n_I + n_{\bar{I}}$, thus leading to $P < 1$. What is much more puzzling is the $P \gg 1$ peak for $\rho_c \simeq \bar{\rho}$. One can only have fluctuations of Q that are larger than those of a dilute gas if the

charges tend to have the same sign. That is to say, what we are seeing is some kind of charge coherence phenomenon: there is some interaction that ensures that charges of a size just less than $\bar{\rho}$ tend to have the same sign. This is in contrast to the evidence we saw in the previous subsection that on the average the nearest neighbour has the opposite sign. We shall examine and resolve this puzzle in the next section.

Is this an artifact of cooling? In Fig.16 we show how $P(\rho_c)$ varies with ρ_c after 46 cooling sweeps. For large and small ρ_c things are much the same as after 23 cools. However the peak near $\bar{\rho}$ has all but disappeared. This indicates that cooling erases this interesting effect: it thus appears that this is a feature of the uncooled vacuum. By comparing comparable plots at different β we find that, as long as the comparison is performed at equivalent numbers of cooling sweeps (in the sense of eqn(21)), this phenomenon seems to roughly scale.

5.3 screening and polarisation

As we have seen, $P(\infty) \ll 1$; i.e. if we include all the charges one finds $\langle Q^2 \rangle \ll \langle n_I + n_{\bar{I}} \rangle$. However we have also seen that if we take the $\sim 50\%$ of the charges with $\rho \leq \bar{\rho}$, then one finds that $\langle Q^2 \rangle > \langle n_I + n_{\bar{I}} \rangle$. This suggests that if we look at $\langle Q^2 \rangle$ as a function of instanton size we will see some dramatic effects. In Fig.17 we plot the value of $\langle Q^2(\rho \leq \rho_c) \rangle$ versus ρ_c , and indeed we do find a dramatic effect: the charge fluctuations for charges with $\rho \leq \bar{\rho}$ are huge compared to the total Q^2 ; about 20 times as large, in the case shown of $\beta = 6.2$ after 23 cools.

What is the origin of this phenomenon? In Fig.17 we see that charges with widths up to $\sim \bar{\rho}$ tend on the average to have the same sign; that is to say their total charge is typically large. However as we include larger charges we see that the typical total charge rapidly becomes much smaller. That is to say: the smaller instantons tend to have the opposite charge to the larger instantons – the former are screened by the latter (and vice-versa).

To highlight this effect we define the following quantity:

$$C(\rho) \equiv \left\langle \frac{Q}{|Q|} \cdot \frac{Q(\rho)}{N(\rho)} \right\rangle. \quad (32)$$

where $Q(\rho)$ is the total topological charge of objects with widths in the bin centered on ρ , and $N(\rho)$ is their corresponding total number. What $C(\rho)$ measures is the correlation of the average charge of instantons of size ρ with the sign of the total charge Q . In Fig.18 we show how $C(\rho)$ varies with ρ . We now see explicitly that the smaller and larger charges tend to have opposite signs and, moreover that it is the smaller charges that tend to have the same sign as Q . What the latter tells us is that the net charge of the smaller charges is greater (in modulus) than the net charge of the larger charges. The large charges are over-screened by the smaller charges. The boundary between ‘large’ and ‘small’ is $\rho \simeq \bar{\rho}$, and scales roughly like a physical quantity when we change β .

To explore this phenomenon further, we calculate for each reference instanton, with width ρ_{ref} , the number of charges within a distance R that have the same sign as the reference charge and whose widths fall into a prescribed range e.g. $\rho > \rho_0$. We call this $N_{same}(R; \rho >$

ρ_0). Similarly for opposite sign charges we have $N_{opp}(R; \rho > \rho_0)$. In Fig.19 we show how $N_{same} - N_{opp}$ varies with ρ_{ref} in the case when we include all the charges, i.e. $R = \infty$ and $\rho > 0$. This is for the $\beta = 6.2$ ensemble after 23 cooling sweeps. We note that total screening corresponds to $N_{same} - N_{opp} = -1$ and a value < -1 indicates over-screening.

The first thing that we observe in Fig.19 is that the smallest instantons are almost completely unscreened; this is what one would expect in a dilute gas and is consistent with the fact that for these values of ρ the quantity $P(\rho_c)$ defined in eqn(31) also shows dilute gas behaviour. As we increase ρ_{ref} we start to see screening. At $\rho_{ref} \simeq \bar{\rho}$ the screening is total and for larger sizes the instantons are overscreened – quite dramatically so for the very largest ones.

As always we have to ask ourselves whether what we see might not be a product of the cooling rather than a property of the uncooled fields. In Fig.20 we show the corresponding plot after 46 cools. Although there is a significant remnant of the under/overscreening that we saw in Fig.19, there is a clear trend towards the much less interesting situation of total screening at all ρ . We conclude that cooling erodes rather than enhances the effect we have found, indicating that it is indeed a property of the original uncooled fields.

In Fig.21 we show what happens when we include in $N_{same} - N_{opp}$ only the smaller charges, i.e. those with $\rho \leq \bar{\rho}$, and if we only count those charges that lie within distances $R = 7, 8, \text{ or } 9$ of the reference charge. Let us first focus on small sizes; say $\rho_{ref} \sim 3$ to 4. We observe from the $R = 7$ data that there is some screening of small charges by other nearby small charges. This is not surprising: overlapping charges can reduce their total action if they can partially annihilate. However we also observe that as we increase R , so including charges that do not significantly overlap with the reference instanton, the screening disappears. This is odd: it tells us that these more distant charges must tend to have the same charge as the reference charge, despite being so far away that one would naively expect very little correlation. If we now turn to the large instantons, we observe that the screening gets rapidly stronger as we increase R ; and indeed that large charges are overscreened by the small charges under consideration here.

Fig.22 is the complement of Fig.21: now $N_{same} - N_{opp}$ includes only the larger charges, i.e. those with widths $\rho \geq \bar{\rho}$. We observe that the screening of small charges by large charges increases as $R \uparrow$; the ‘normal’ screening behaviour. Indeed if we go to large R it is clear from these two figures that the screening of small charges is entirely driven by the large charges. For large ρ_{ref} the situation is entirely different: large charges are strongly antiscreened by other large charges i.e. these quite strongly overlapping large charges tend to have the same sign.

Again we find that all these effects weaken with increasing cooling suggest that they are properties of the original uncooled fields.

We now have enough information to hazard a model of the topological structure that embodies all these features. We think of the vacuum as being composed of small and large charges. Small charges are superimposed on the broad backs of the large charges because the latter are everywhere: they densely pack Euclidean space-time. The small charges will tend to have the opposite sign to the large charge in which they are embedded and so, except when they are close enough for their mutual overlap to outweigh this effect, will tend to have the

same sign as each other. At the same time broad charges overlap so these small charges will be simultaneously embedded in more than one broad charge. They will thus tend align the charges of such overlapping broad charges. So we have a picture of the broad charges tending, on the average, to have the same sign throughout the vacuum and the small charges also having the same sign as each other on the average but opposite to that of the broad charges. This is driven by the mutual interaction of the small, mutually non-overlapping charges with the large, mutually overlapping charges. The net charge is that of the smaller charges because, since they overlap less, their charge polarisation is stronger.

This picture of the charge structure of the vacuum goes somewhat beyond what our numerical evidence demands but seems plausible. Presumably some of the observed breakdown of our naive screening intuition is not surprising: it arises from the fact that while the latter is based on a $\propto 1/r$ potential between pointlike charges, the effective potential here will have a more complicated form when the charges overlap, and will fall much more rapidly with r when they do not.

Although it is not possible to simply guess at the consequences of these non-trivial long-range charge correlations for light quark physics, it would be surprising if there were none.

6 Topological susceptibility

While the identification of the topological structure of the vacuum is, as we have seen, a complicated and sometimes ambiguous task, the total topological charge, Q , is quite straightforward to extract. Moreover as we saw in the Introduction, this quantity is related to the masses of the pseudoscalar mesons via eqn(1). Although it was not the primary purpose of our calculations, we have accumulated values of $\langle Q^2 \rangle$ and hence of the susceptibility χ_t over the range $6.0 \leq \beta \leq 6.4$. Our statistics is not very high but we do get closer to the continuum limit than any other calculation that we are aware of. It is therefore worthwhile extracting a prediction for χ_t in physical units.

There are various ways one can manipulate the raw, non-integer lattice topological charge so as to obtain an estimate of the ‘true’ integer topological charge of the field configuration. These definitions will differ by lattice corrections which should vanish as $a \rightarrow 0$. In Table 11 we show our calculated values of the susceptibility using two such definitions. The first, Q_L , is simply the integral of the lattice topological charge density rounded to the nearest integer. The second, Q , is our best estimate of the integer topological charge, obtained by applying lattice corrections as described in the Appendix and then rounding to the nearest (and usually nearby) integer. We obtain the susceptibility in lattice units, $a^4\chi_t$, if we divide $\langle Q^2 \rangle$ by the volume in lattice units; and similarly $a^4\chi_{t,L}$ from $\langle Q_L^2 \rangle$. Since these quantities differ by lattice corrections, they should possess a common continuum limit. This is something we shall investigate below.

The first thing we observe is that if there is any variation with the number of cooling sweeps it is much less than the statistical error and so can be ignored. We also note that the two lattice sizes at $\beta = 6.0$ give susceptibilities that are within 2σ of each other. We take this as evidence of no significant finite-volume effects. Finally we remark that the $\beta = 6.4$

ensemble consists of only 20, albeit well-separated, field configurations and so one should treat the corresponding error estimate with some caution.

Using the values for the string tension in eqn(18) we can form the dimensionless mass ratio $\chi_t^{1/4}/\sqrt{\sigma}$. In Fig. 23 we plot $\chi_t^{1/4}/\sqrt{\sigma}$ against the string tension in lattice units, $a^2\sigma$. We expect the leading lattice corrections to this dimensionless mass ratio to be $O(a^2)$ [24], so we can attempt a continuum extrapolation of the form

$$\frac{\chi_t^{1/4}(a)}{\sqrt{\sigma(a)}} = \frac{\chi_t^{1/4}(0)}{\sqrt{\sigma(0)}} + ca^2\sigma \quad (33)$$

This will be a simple straight line in our Figure. As we see the calculated values are consistent with this functional form. In addition to the susceptibility calculated from $\langle Q^2 \rangle$ we show the susceptibility calculated from $\langle Q_L^2 \rangle$. In Table 12 we show the continuum values of the these ratios, together with earlier [20] results obtained over the range $5.7 \leq \beta \leq 6.2$. We see that all the results are entirely consistent with each other.

To obtain χ_t in physical units, we use the value for $\sqrt{\sigma}$ in eqn(19). Substituting this value we obtain

$$\chi_t^{1/4} = 187 \pm 14 \pm 16 MeV \quad (34)$$

where the second error reflects the uncertainty in assigning a value to the string tension in MeV units. This, we note, is in satisfactory agreement with our expectations from eqn(1).

7 Conclusions

The influence of topological structure on the physics of QCD arises most directly from the near-zero modes that it induces in the $\mathcal{D}[A]$ quark operator. Without performing the appropriate eigenvalue calculations on the fields it is not possible to be certain which aspects of that structure are physically important and which are not. For example, suppose that the broader instantons belonged entirely to strongly overlapping $I\bar{I}$ pairs. In that case they would not contribute small modes to $\mathcal{D}[A]$ and so would be essentially irrelevant. As we have seen, the smaller instantons form an approximate dilute gas. Such a dilute gas is what is assumed in the Instanton Liquid Model [4] and so in that case our apparently very different topological structure would in fact be consistent with that model.

Given that we do not, in this paper, calculate the contribution of the topological structure to quark propagators and hadron physics, it has seemed to us that the sensible approach is to expose all the structure that is there without any prejudice as to what might be important or not.

Exposing the topological structure is a non-trivial task. First one needs to separate the uninteresting high-frequency modes from the interesting modes on physical length scales. We have chosen to use the ‘cooling’ technique; and we performed some studies to find the variant which appeared to distort the interesting long-distance structure the least. There are other approaches [16, 15] and the relationship between all these methods needs to be better understood; particularly as they appear to lead to significantly different results.

Secondly one needs to categorise the topological structure in some useful way. We have decomposed it into topological charges of various sizes and locations. To do so requires a rather complicated pattern-recognition algorithm. Although we have tested the robustness of this algorithm to small variations within the general scheme, this can only be a first step in exploring its reliability.

It is of course not at all certain that the topological structure of the uncooled fields can be usefully described in terms of (overlapping) charges that are localised within some width ρ of a particular location. While there is some evidence from older calculations that instanton collective coordinates are the appropriate degrees of freedom to use, this really needs a much more careful study. Cooling will, of course, deform the field into such a superposition of charges and so it makes sense to perform the analysis in these terms on the cooled fields. One might take the sophisticated point of view that even if the uncooled topological structure is not really a superposition of approximately classical charges, cooling provides us with the distribution of the latter charges that most closely reproduces the true structure - and hence its physics as well. This would then be the appropriate way to test the assumptions of instanton models.

In any case, it is clear that one must always check how robust under cooling are any conclusions that one wishes to draw. This is something we have attempted to do. The fact is that there is indeed a significant variation under cooling for many quantities and this introduces some uncertainty into how one should interpret the calculated values. Unfortunately our ‘pattern recognition’ algorithms must break down as $n_c \rightarrow 0$ (because of the increase in the apparent density) and so we are not able to attempt an extrapolation to $n_c = 0$. In this paper we have focussed on developing techniques to reveal the structure of the cooled fields: the problem of how precisely this relates to the uncooled fields still awaits a convincing resolution.

At the same time, because the separation between ultraviolet and physical frequencies is approximate, but improves as $a \rightarrow 0$, it is important to perform scaling studies whenever possible. This we have also done: the numbers we quote here for the mean size, density etc. are the values that one obtains after an extrapolation to the continuum limit. Finally, we have explicitly checked that any finite-volume effects are essentially within our statistical errors.

The simplest quantity to calculate, and one to which many of the above caveats do not apply, is the topological susceptibility, χ_t . Our calculation goes to smaller values of a than any previous SU(3) calculation and confirms previous claims that eqn(1) is well satisfied; indeed, better than one could expect.

The topological charge distribution we obtain is characterised by a mean width $\bar{\rho} \simeq 0.56(5)fm$, which is significantly larger than that which is typically assumed in Instanton Liquid Model calculations [4]. The average separation between nearest neighbour charges is comparable to the average width: so the vacuum is densely packed.

The distribution is quite broad: the full-width is $2\sigma_\rho \simeq 0.22(2)fm$. Our fits to the small- ρ tail of this distribution do show some signs of a trend for it to approach the predicted $D(\rho) \propto \rho^6$ behaviour when β is increased and when the number of cooling sweeps is reduced, but the evidence for this is rather rough. At large- ρ we find a rapid fall-off that can be represented by something like $D(\rho) \propto 1/\rho^{11}$. This is much more severe than the $1/\rho^5$ behaviour that one

might argue on the basis of a coupling that freezes at large distances.

The values of $\bar{\rho}$ and σ_ρ appear to become smaller as the number of cooling sweeps is decreased. However it is not clear whether this is a real effect or whether it is a reflection of the increasing unreliability of our pattern recognition algorithms in the denser vacuum at smaller n_c . Neither is it clear how pronounced this effect would be after extrapolation to the continuum limit.

We have found an interesting pattern of correlations amongst the instantons. As expected, nearest neighbour charges are more likely to have opposite signs. There seems to be, in addition, something like a ‘hard core’ repulsion: instantons very close to each other are suppressed much more than one would expect on the simple basis of phase space. Very small instantons do behave like a dilute gas, but the bulk of charges with $\rho < \bar{\rho}$ do not. Instead they seem to have charges that are biased, on the average, towards being the same. Thus the fluctuations in topological charge, when restricted to sizes less than the mean, are hugely amplified: $\langle Q^2(\rho < \bar{\rho}) \rangle \gg \langle Q^2 \rangle$. At the same time the very large charges also tend to have the same sign, and this is opposite to that of the smaller instantons. It is the charge of the smaller instantons that is the greater (in modulus) and they determine the sign of Q . So the smaller instantons are (under)screened by the larger instantons; and the larger instantons are (over)screened by the smaller instantons. That is to say, the vacuum has a long-range charge coherence that depends on the scale. This effect becomes more pronounced as the number of cools is decreased and so it seems reasonable to infer that it is a real property of the uncooled vacuum.

We recall that topological charge fluctuations are physically important; e.g they play an important role in generating the η' mass. For this reason the effect we have identified might well have an impact on the physics. In particular if a quantity were sensitive to fluctuations in Q but, for some dynamical reason, was insensitive to $\rho > \bar{\rho}$ (or the reverse), then it would be affected far more strongly than if one simply used the total Q^2 as a measure of the relevant fluctuations. However to go further along these lines one really needs to consider the fermionic physics in the background of these fields; a topic that lies beyond the scope of this paper.

Acknowledgements

DS would like to thank Hubert Simma for many useful discussions. The work of DS was supported by the Carnegie Trust, the UKQCD travel grant from PPARC, and by computing grants, for T3D and J90 time, from PPARC and the University of Edinburgh. MT has been supported by PPARC grants GR/K55752 and GR/K95338. Both DS and MT thank the Newton Institute for hospitality during part of this work, and DS also thanks Oxford Theoretical Physics for its hospitality on various occasions.

Appendix

In this Appendix we go briefly into some of the details that it would have been tedious to leave in the main body of the text.

(a) lattice corrections to Q_L

The lattice topological charge $Q_L = \int Q_L(x)dx$ of an instanton will not be exactly unity, but, as we see in eqn(8), will suffer $O(a^2)$ corrections. The relevant scale is ρ and so if this is expressed in lattice units, we have

$$Q_L = 1 + \frac{c}{\rho^2} + O\left(\frac{1}{\rho^4}\right) \quad (35)$$

Such corrections are relevant in several parts of our calculations. For example, we tune our filters so as to minimise the discrepancy $\delta_Q = |Q - (n_I - n_{\bar{I}})|$. If we use $Q = Q_L$ this may introduce a significant error. Another example concerns the topological susceptibility: $\langle Q_L^2 \rangle$ will differ from $\langle Q^2 \rangle$ and it is the latter that we want. Since we determine the widths of all the charges in each field configuration, we can easily correct for all the lattice artifacts once we have determined the coefficients in the expression in eqn(35).

To determine $Q_L(\rho)$ for a single instanton, we take a large discretised instanton on a very large lattice and cool it. As we cool it, it will gradually shrink. (Recall that we use a plaquette ‘action’ to drive the cooling.) As it shrinks we calculate Q_L and ρ ; we then find that we can fit these with the simple form:

$$Q_L = 1 - \frac{0.65}{\rho^2} - \frac{5.344}{\rho^4} \quad (36)$$

This heuristic fit is in practice only needed down to $\rho \sim 2$, and for that it is adequate.

There is one important detail we have skated over. How does one determine the value of ρ that is used in eqn(36)? This is intrinsically ambiguous since the shape of a small lattice instanton differs qualitatively from the continuum shape. It should however be apparent that this ambiguity does not matter; the role of ρ is simply to act as a label parametrising instantons of different sizes. What is important is that once we pick some definition of ρ , we then use it consistently throughout our calculations.

A simple way to define ρ is to use a continuum relation between some aspect of the instanton topological charge density and its width. For example, we could use the relation between Q_p and ρ as given in eqn(12). On the lattice we would calculate $Q_{L,p}$ and then use this relation to define ρ for us. This might be improved by replacing Q_p with $Q_{L,p}/Q_L$ in eqn(12). (To avoid the double-valuedness that potentially arises when $\rho \sim 1$.) In practice we have chosen to use a different relation. We recall that for a continuum instanton the total topological charge within a distance ρ of the centre is $1/2$. We therefore define ρ for our lattice instanton to be the distance within which it contains a topological charge of $Q_L/2$. This is used throughout our calculations. Of course the discrete nature of the lattice means that one has to make some particular choices as to how to implement this criterion. (There are some unsatisfactory features in the choices we actually made – but in practice, because really small instantons are very rare, these do not matter.)

As we increase β , the number of instantons small enough for these corrections to be important rapidly decreases and so, as long as one performs a scaling study, all methods lead to equivalent results.

(b) lattice correction to Q_p

The continuum expression for Q_p in eqn(12) will also have $O(a^2)$ lattice corrections. The scale for these is set by ρ and so, if ρ is expressed in lattice units, such a correction corresponds to an extra term of $O(1/\rho^6)$. To determine the corrections we cooled a classical instanton, calculating ρ as described above. The resulting relationship between the peak lattice topological charge and ρ may be parameterised as

$$Q_{L,p} = \frac{6}{\pi^2 \rho^4} \left(1 - \frac{1.962}{\rho^2} + \frac{1.198}{\rho^3} \right). \quad (37)$$

We have included a heuristic $1/\rho^3$ correction to mimic all the higher (even) powers that will become important at very small ρ . Eqn(37) has been used in this paper for calculating ρ from the peaks.

(c) lattice correction to $Q(|\mathbf{x}| \leq R)$

In our filters we have used the topological charge within a distance ρ to define a width, ρ_R . This is then compared to the width calculated from the peak. The continuum expression for $Q(|x| \leq R)$ is given in eqn(16). For small ρ this will need lattice corrections and these can be found just as for Q_p . For example, for the case $R = 2$ which we use in practice in our filters, we find that one can parametrise the lattice corrections by

$$Q_L(|x| \leq 2) = Q(|x| \leq 2) \left(1 - \frac{1.66}{\rho^2} - \frac{1.26}{\rho^4} \right). \quad (38)$$

This can then be used to extract a width, $\rho_2 \equiv \rho$, for each peak in the vacuum and this can be used in the filters. (In fact we used a slightly different, but considerably less elegant, functional form which is essentially the same for the values of ρ that arise in practice.)

References

- [1] S. Coleman, Aspects of Symmetry, Ch.7 (CUP 1985).
- [2] G. 't Hooft, Physics Reports 142 (1986) 357.
- [3] D. Diakonov, Lectures at the *1995 Enrico Fermi School*, hep-ph/9602375.
- [4] T. Schaefer and E. Shuryak, hep-ph/9610451.

- [5] S. Hands and M. Teper, Nucl. Phys. B347 (1990) 819.
- [6] N. Dowrick and M. Teper, Nucl. Phys. Proc. Suppl. B42 (1995) 237.
- [7] T. Yoshie, Plenary Review at *Lattice 97*, hep-lat/9711017.
- [8] E. Witten, Nucl. Phys. B156 (1979) 269.
- [9] G. Veneziano, Nucl. Phys. B159 (1979) 213.
- [10] J. Hoek et al, Nucl. Phys. B288 (1987) 589.
- [11] M. Teper, Phys. Lett. B202 (1988) 553.
- [12] M. Campostrini et al, Phys. Lett. B212 (1988) 206; B. Alles, M. D'Elia and A. Di Giacomo, Nucl. Phys. B494 (1997) 281.
- [13] C. Michael and P. Spencer, Phys. Rev. D52 (1995) 4691.
- [14] R. Brower et al, Nucl. Phys. Proc. Suppl. 53 (1997) 547.
- [15] T. DeGrand, A. Hasenfratz and T. Kovacs, hep-lat/9705009; hep-lat/9711032.
- [16] Ph. de Forcrand, M. Perez and I. Stamatescu, Nucl. Phys. B499 (1997) 409.
- [17] H. Simma, D. Smith and M. Teper, hep-lat/9709128.
- [18] Ph. de Forcrand et al, hep-lat/971001.
- [19] A. Hasenfratz, private communication.
- [20] M. Teper, Lectures at the Newton Institute NATO-ASI School, June 1997, hep-lat/9711011.
- [21] P. di Vecchia et al, Nucl. Phys. B192 (1981) 392.
- [22] M. Teper, Phys. Lett. B162 (1985) 357.
- [23] C. Michael and M. Teper, Nucl. Phys. B314 (1989) 347. G.Bali et al, Phys. Lett. B309 (1993) 378. Ph.de Forcrand et al, Phys. Lett. B160 (1985) 137; P. Bacilieri et al, Phys. Lett. B205 (1988) 535; S. Perantonis and C. Michael, Nucl. Phys. B347 (1990) 854; G. Bali and K. Schilling, Phys. Rev. D46 (1992) 2636; Phys. Rev. D47 (1993) 661; S. Booth et al, Nucl. Phys. B294 (1992) 385; C. Allton et al, Nucl. Phys. B407 (1993) 331; H. Wittig, Nucl. Phys. Proc. Suppl. B42 (1995) 288.
- [24] K. Symanzik, Nucl. Phys. B226 (1983) 187.

cools	$\langle \delta_Q \rangle$	$\sqrt{\langle Q^2 \rangle}$	$\langle N_{tot} \rangle$
23	12.45	4.1	493.8
32	10.39	4.0	273.6
46	7.08	4.0	151.1

Table 1: Mismatch, δ_Q , typical total charge, $\sqrt{\langle Q^2 \rangle}$, and total number of charges: against number of cooling sweeps at $\beta = 6.2$.

β	cools	ϵ_2	ρ_c	ϵ_c	δ_Q
6.0	23	0.19	6.84	0.20	2.90
	28	0.17	6.50	0.25	2.25
	32	0.11	8.46	0.20	2.75
	46	0.10	16.00	0.10	1.70
large	46	0.10	6.89	0.25	6.25
6.2	23	0.27	7.80	0.30	4.40
	32	0.20	6.83	0.25	3.55
	46	0.11	9.31	0.20	2.25
6.4	30	0.24	10.89	0.20	4.00
	50	0.21	9.43	0.30	2.80
	70	0.10	11.25	0.30	1.83
	80	0.05	10.83	0.15	1.92

Table 2: The filter parameters used in this paper, with corresponding charge mismatch, δ_Q .

cools	ϵ_3	ρ_c	ϵ_c	δ_Q
23	0.62	7.60	0.3	3.65
32	0.46	6.83	0.25	3.85
46	0.24	7.18	0.20	1.90

Table 3: Filter parameters for $\beta = 6.2$, using ρ_3 in the filter

cools	#peaks (unfiltered)	#peaks (ρ_2)	#peaks (ρ_3)
23	540	495	489
32	302	271	267
46	164	158	148

Table 4: Number of peaks, at $\beta = 6.2$, before and after applying filters based on ρ_2 and ρ_3 respectively.

cools	#peaks in $Q(x)$	#peaks in $S(x)$	R	#peaks with $ x_{action} - x_{charge} \leq R$
23	168	95	0	54
23	168	95	$\sqrt{2}$	86
46	63	46	0	33
46	63	46	$\sqrt{2}$	43

Table 5: Number of peaks in $S(x)$ that can be indentified with a peak in $Q(x)$.

β	cools	$\bar{\rho}$	σ_ρ	$\langle N_{tot} \rangle$	$\langle N_{tot} \rangle / V$
6.0	23	5.25(1)	1.20(4)	147.5	0.328(8)
	28	5.40(2)	1.29(5)	113.0	0.251(6)
	32	5.43(2)	1.36(5)	86.2	0.192(5)
	46	5.65(2)	1.51(6)	57.5	0.128(3)
large	46	5.63(1)	1.51(3)	613.6	0.128(3)
6.2	23	6.41(1)	1.17(3)	493.8	1.112(28)
	32	6.94(1)	1.35(4)	273.6	0.616(15)
	46	7.44(2)	1.57(5)	151.1	0.340(9)
6.4	30	7.86(1)	1.32(5)	1005.3	2.195(82)
	50	9.00(2)	1.61(8)	369.7	0.807(30)
	70	9.70(4)	1.92(11)	205.2	0.448(17)
	80	9.84(5)	2.04(12)	156.6	0.342(13)

Table 6: Average and width of size distribution; also the total number of charges and the number per unit physical volume.

cools	$\bar{\rho}$	σ_ρ	$\langle N_{tot} \rangle$	f
20	6.92	1.29	2177	15.6
30	7.96	1.52	1063	13.1
40	8.74	1.95	604	12.0
50	9.27	1.98	395	9.1
60	9.70	2.23	286	26.2
70	10.06	2.27	224	22.8

Table 7: Variation with cooling, n_c , of a single configuration at $\beta = 6.4$ prior to any filtering.

β	cools	range	γ_s
6.0	23	0.44-0.77	3.3(2)
6.0	28	0.44-0.99	3.1(1)
6.0	32	0.44-0.77	2.9(2)
6.0	46	0.44-0.99	2.6(1)
6.2	23	0.48-0.72	6.9(2)
6.2	32	0.48-0.88	5.4(2)
6.2	46	0.48-0.72	4.8(3)
6.4	30	0.55-0.73	9.2(4)
6.4	50	0.55-0.97	5.7(2)
6.4	70	0.55-0.97	4.7(3)
6.4	80	0.61-1.03	4.0(3)

Table 8: Fits to the small- ρ tails of the size distributions. The range fitted is in units of $1/\sqrt{\sigma}$.

β	cools	range	γ_l
6.0	23	1.43-1.87	11.2(4)
6.0	28	1.54-2.20	10.8(4)
6.0	32	1.54-2.20	10.1(4)
6.0	46	1.65-2.31	10.0(5)
6.2	23	1.20-1.44	11.9(3)
6.2	32	1.36-1.68	11.9(3)
6.2	46	1.44-2.00	10.2(3)
6.4	30	1.09-1.46	11.0(3)
6.4	50	1.46-1.64	12.2(2)
6.4	70	1.52-1.64	10.0(2)
6.4	80	1.46-1.82	10.4(8)

Table 9: Fits to the large- ρ tails of the size distributions. The range fitted is in units of $1/\sqrt{\sigma}$.

β	cools	$\bar{R}_{like}\sqrt{\sigma}$	$\bar{R}_{unlike}\sqrt{\sigma}$
6.0	23	1.072(6)	0.931(6)
6.0	28	1.152(7)	1.008(6)
6.0	32	1.233(8)	1.077(7)
6.0	46	1.359(9)	1.223(9)
6.2	23	0.791(5)	0.700(5)
6.2	32	0.935(6)	0.818(6)
6.2	46	1.075(7)	0.958(7)
6.4	30	0.667(6)	0.604(6)
6.4	50	0.884(7)	0.775(8)
6.4	70	1.013(11)	0.911(9)
6.4	80	1.080(12)	0.976(10)

Table 10: Average distance to nearest charge of the same and opposite sign; in units of $1/\sqrt{\sigma}$.

β	cools	$\langle Q_L^2 \rangle$	$\langle Q^2 \rangle$
6.0	23	14.4(2.0)	18.8(2.8)
6.0	28	15.0(2.0)	18.6(2.6)
6.0	32	15.1(2.1)	18.5(2.6)
6.0	46	15.7(2.1)	17.9(2.6)
large	46	97.3(18.6)	120.2(23.1)
6.2	23	14.1(2.0)	17.1(2.6)
6.2	32	14.5(2.1)	16.1(2.4)
6.2	46	15.2(2.2)	16.0(2.4)
6.4	30	16.4(6.6)	17.4(7.1)
6.4	50	17.4(7.1)	17.4(7.1)
6.4	70	17.4(7.1)	17.4(7.1)
6.4	80	17.4(7.1)	17.4(7.1)

Table 11: Average values of Q^2 for corrected (Q) and uncorrected (Q_L) chrges respectively.

$\chi_t^{1/4}/\sqrt{\sigma}$	$\chi_{t,L}^{1/4}/\sqrt{\sigma}$	$\chi_{t,old}^{1/4}/\sqrt{\sigma}$
0.424(32)	0.437(34)	0.437(25)

Table 12: Continuum limit of susceptibility in units of the string tension: for corrected (χ_t) and uncorrected ($\chi_{t,L}$) charges; and a previous calculation [20] for comparison.

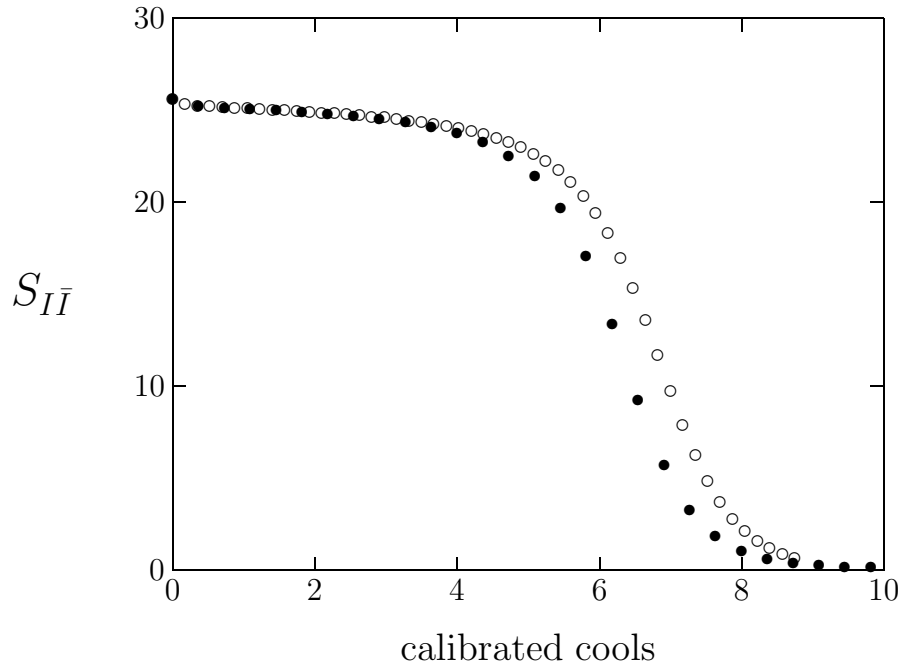


Figure 1: Action of $I\bar{I}$ pair against number of calibrated cooling sweeps, for $\alpha = 0$ (\bullet) and $\alpha = 2$ (\circ).

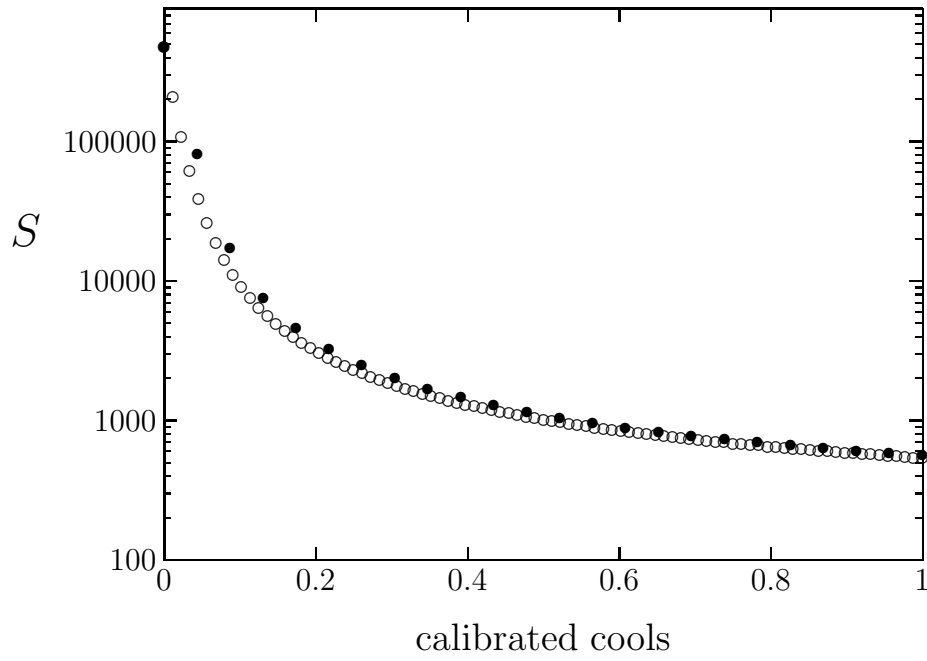


Figure 2: Action against number of calibrated cooling sweeps, for $\alpha = 0$ (\bullet) and $\alpha = 2$ (\circ).

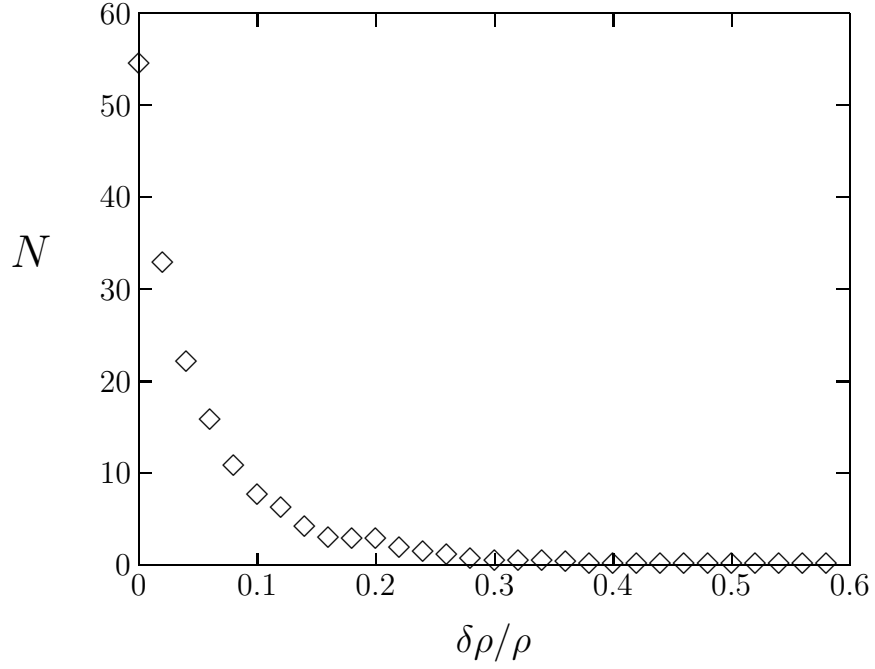


Figure 3: Number of times a given fractional change in width occurs when using eqn(13): at $\beta = 6.0$ after 23 cools.

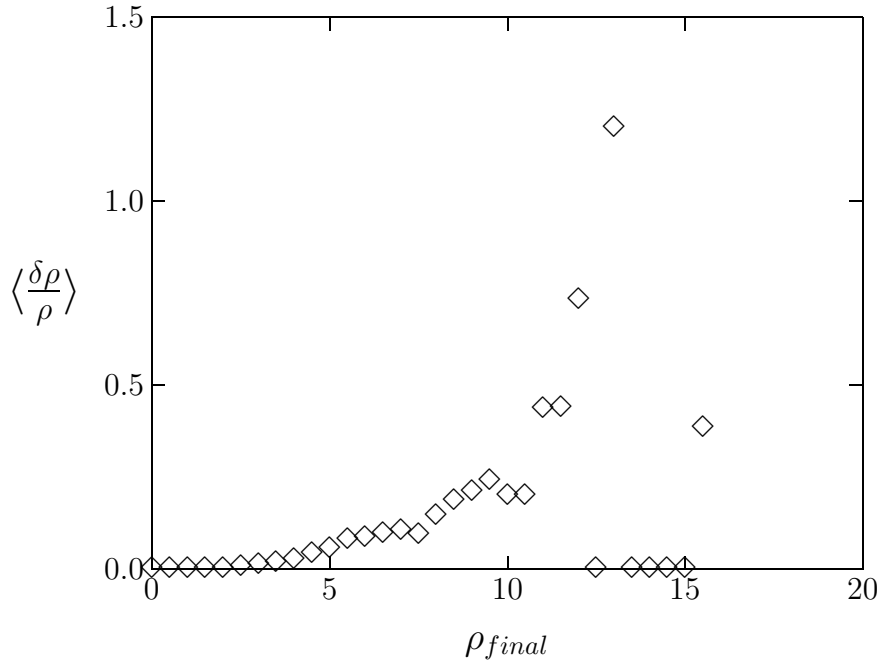


Figure 4: Fractional change in width, against the final width, after using eqn(13) to account for presence of other charges: at $\beta = 6.0$ after 23 cools.

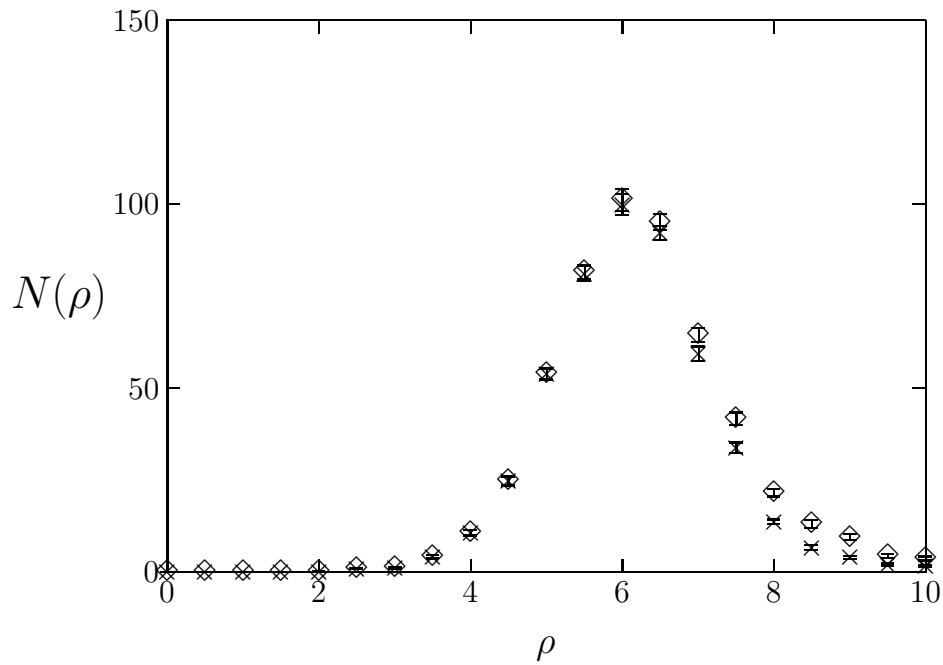


Figure 5: Filtered (\times) and unfiltered (\diamond) size distributions after 23 cooling sweeps at $\beta = 6.2$.

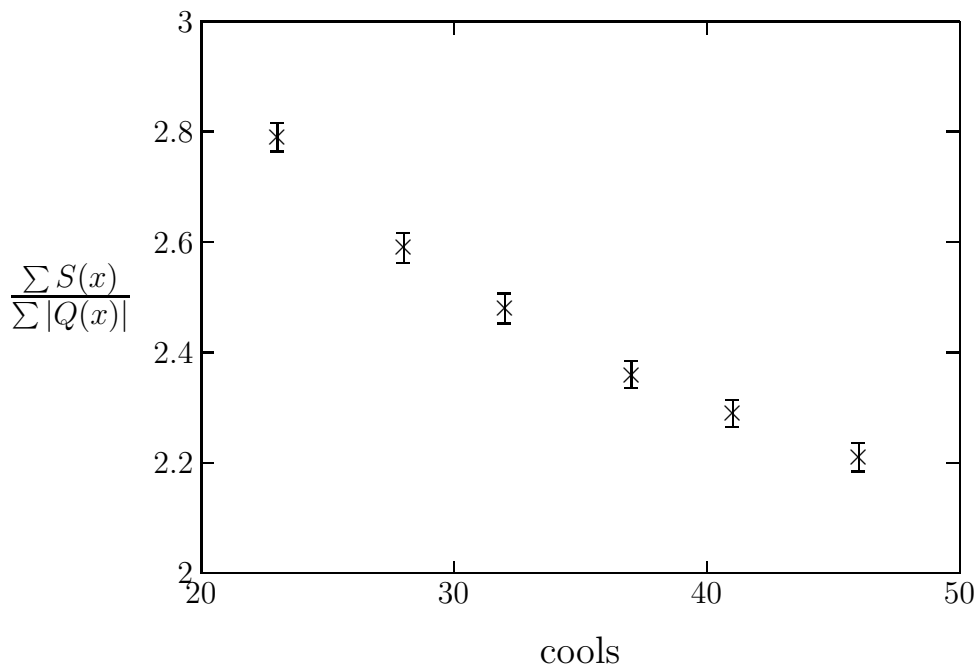


Figure 6: $\frac{\sum_x S(x)}{\sum_x |Q(x)|}$ against number of cooling sweeps, at $\beta = 6.0$.

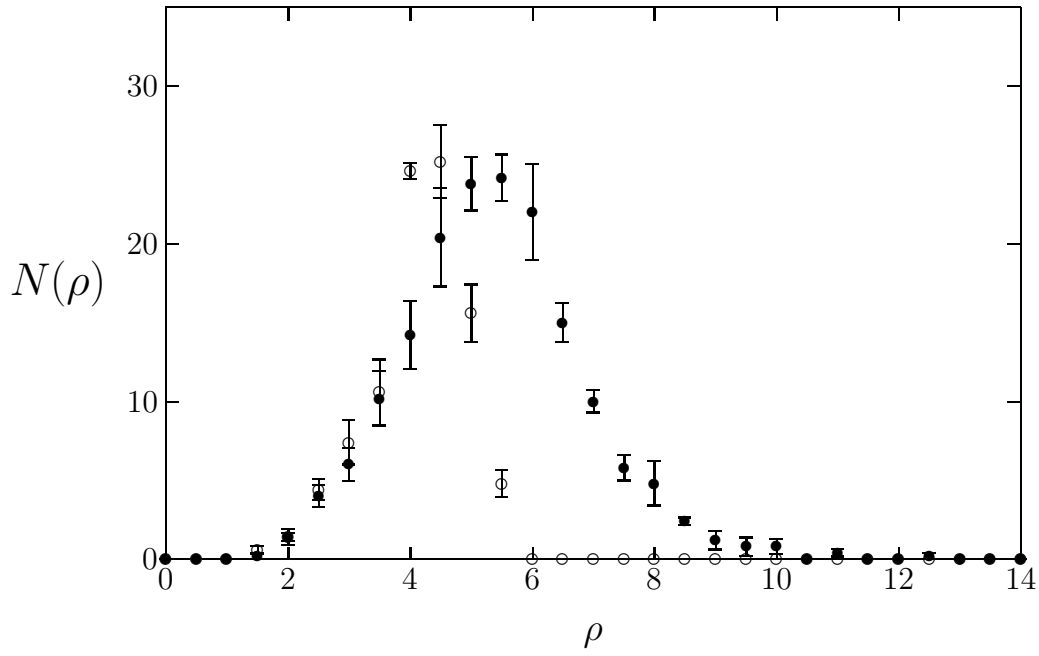


Figure 7: Size distributions from $S(x)$ (\circ) and from $Q(x)$ (\bullet) after 23 cooling sweeps at $\beta = 6.0$.

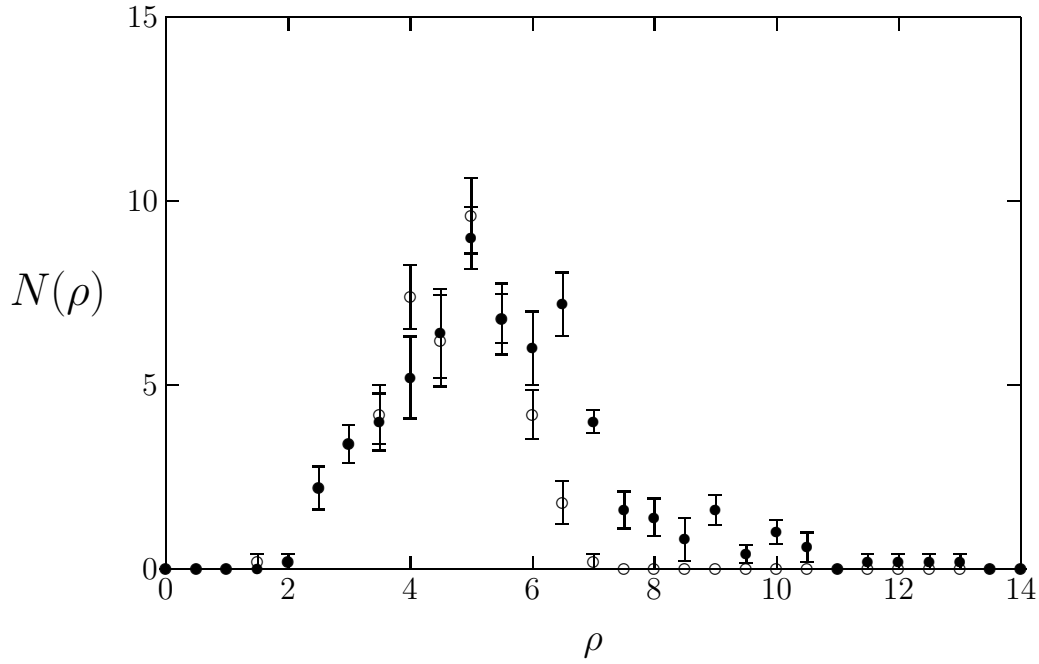


Figure 8: Size distributions from $S(x)$ (\circ) and from $Q(x)$ (\bullet) after 46 cooling sweeps at $\beta = 6.0$.

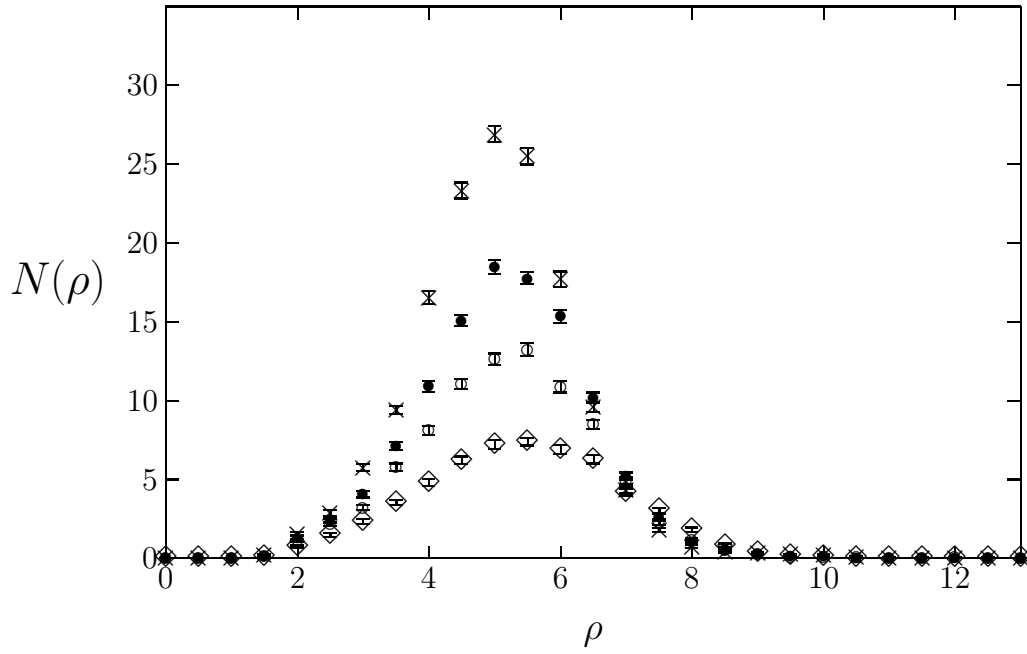


Figure 9: The number of charges of different sizes; at $\beta = 6.0$ for 23(\times), 28(\bullet), 32(\circ) and 46(\diamond) cools.

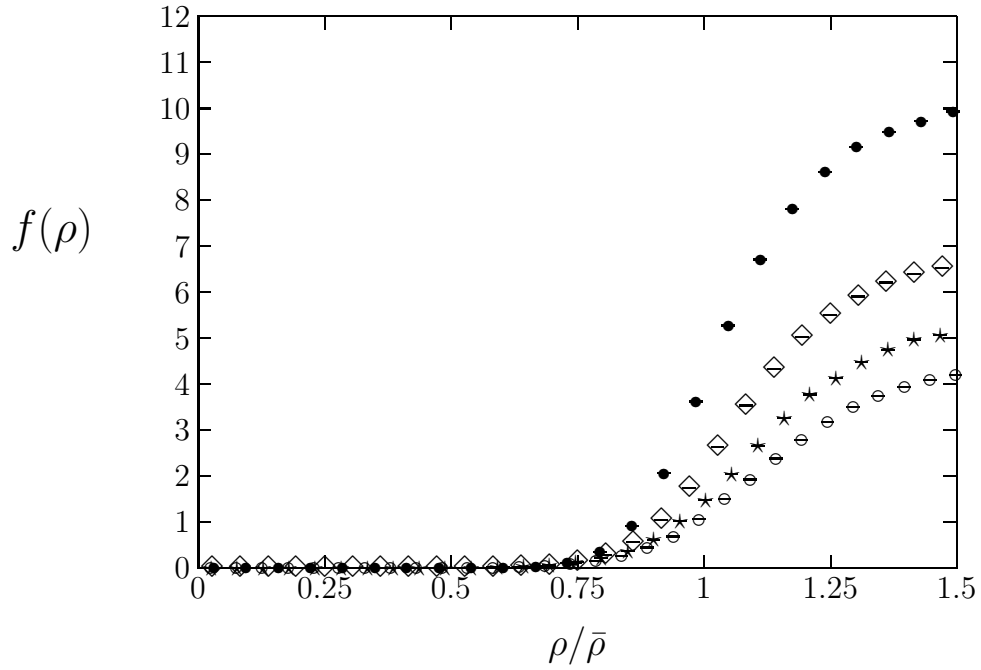


Figure 10: Packing fraction of instantons of size $\leq \rho$ against ρ in units of $\bar{\rho}$. For 30(\bullet), 50(\diamond), 70(\star) and 80(\circ) cooling sweeps at $\beta = 6.4$.

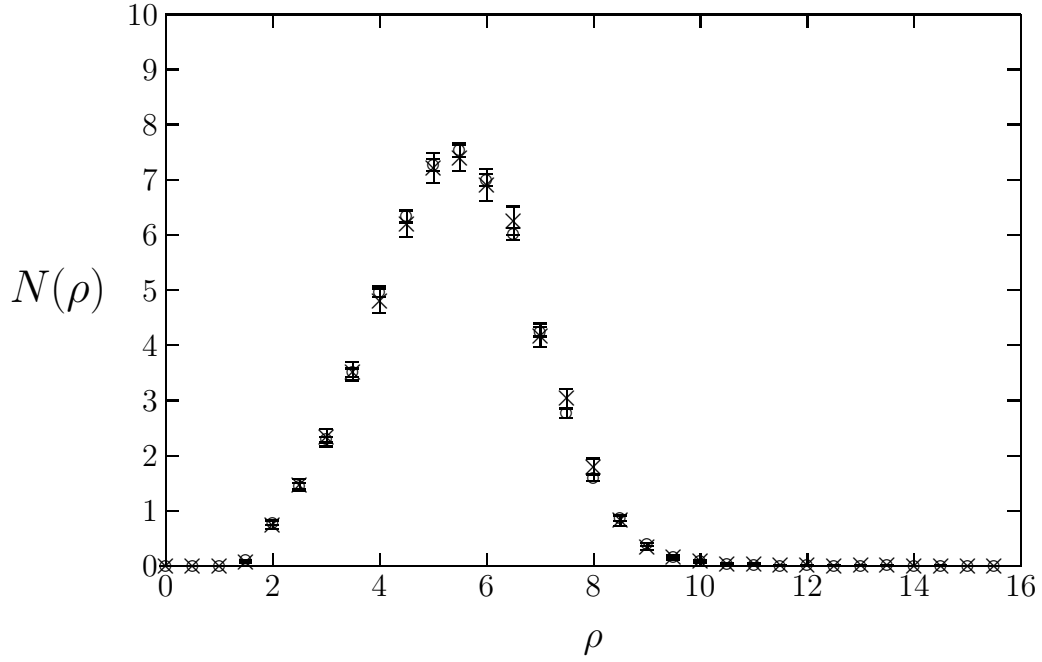


Figure 11: Comparison of size distributions on 16^{348} (\times) and 32^{364} (\circ) lattices at $\beta = 6.0$ after 46 cools.

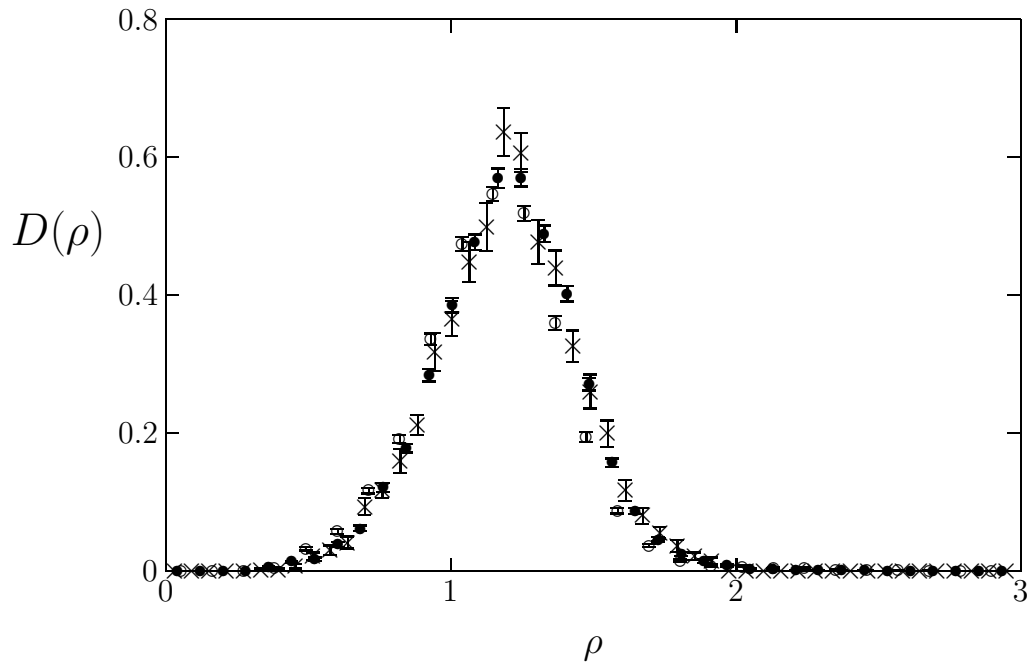


Figure 12: Density of charges against ρ : at $\beta = 6.0$ after 23 cools (\circ), at $\beta = 6.2$ after 46 cools (\bullet) and at $\beta = 6.4$ after 80 cools (\times). All in physical units of $1/\sqrt{\sigma}$.

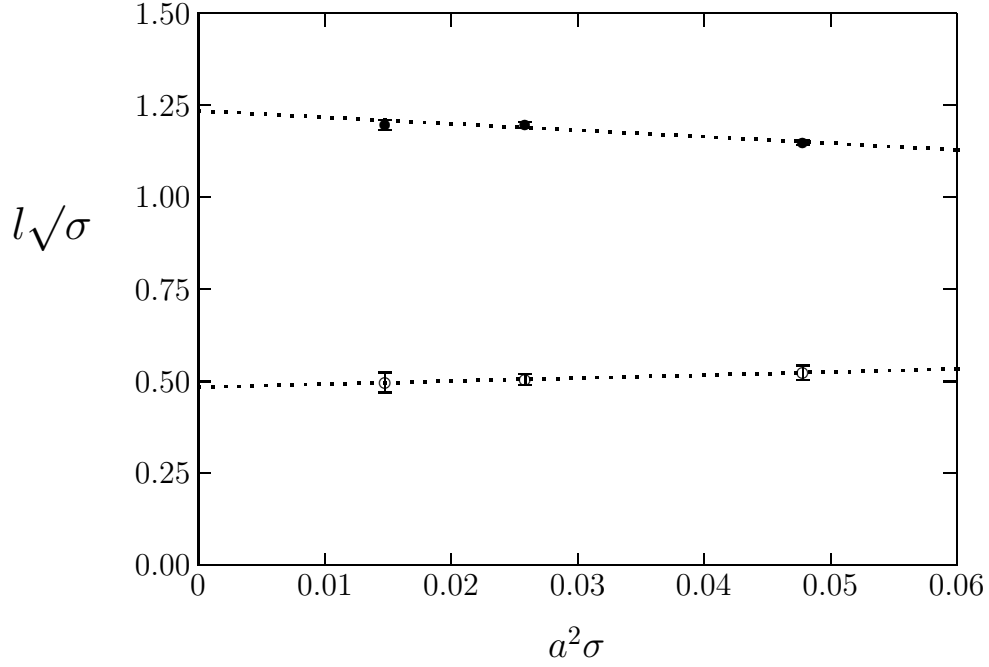


Figure 13: Average, $l = \bar{\rho}(\bullet)$, and full-width, $l = 2\sigma_\rho(\circ)$, of the instanton size distributions. Lines are continuum extrapolations.

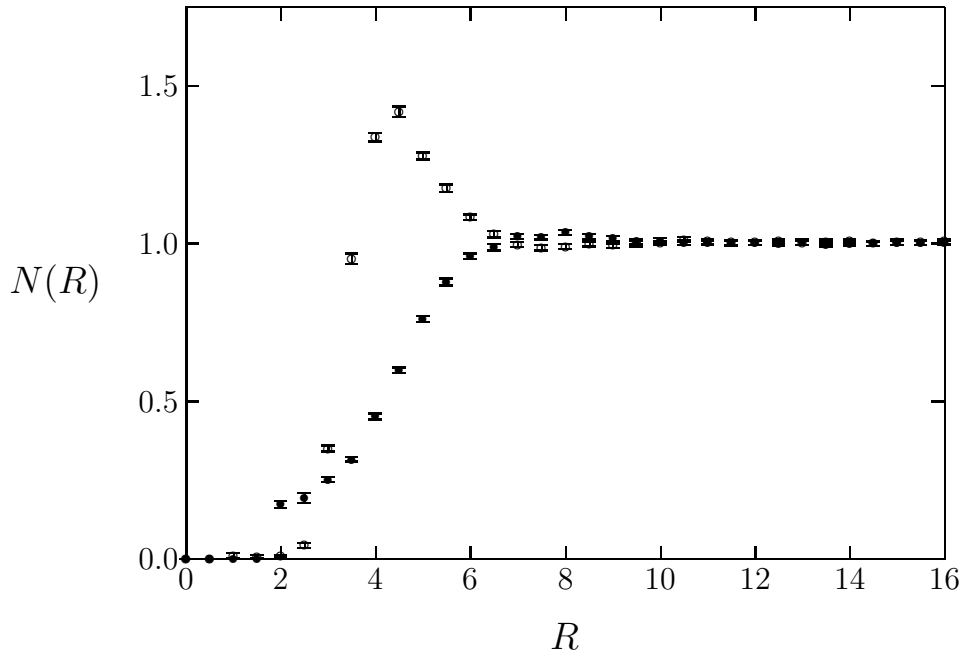


Figure 14: Number of same sign (\bullet) and opposite sign (\circ) charges, per unit volume, as a function of distance R from the reference charge. At $\beta = 6.2$ after 23 cooling sweeps.

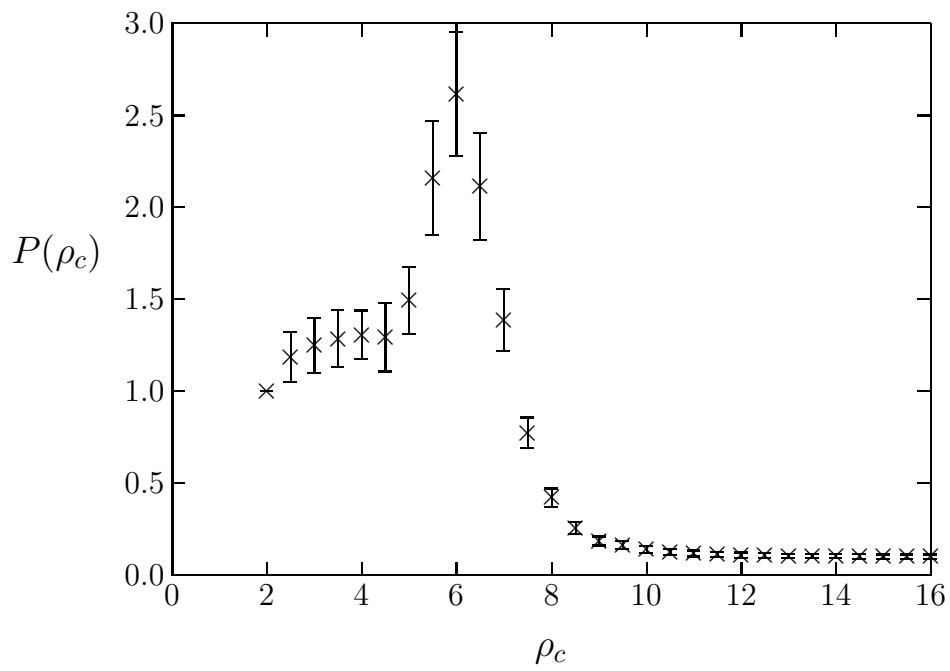


Figure 15: $P(\rho_c)$, as defined in eqn(31), versus ρ_c at $\beta = 6.2$ after 23 cools.

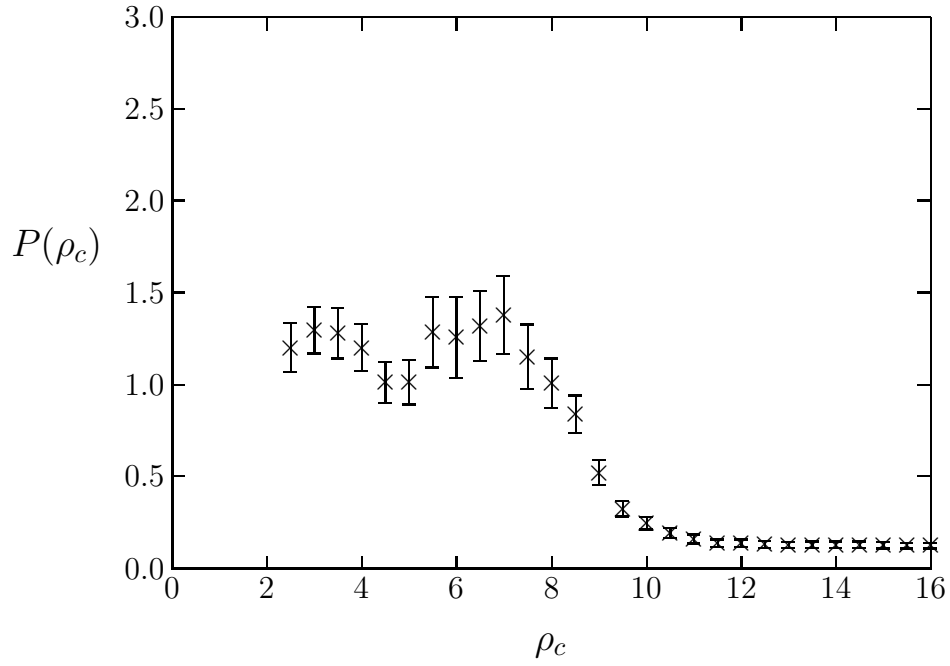


Figure 16: $P(\rho_c)$, as defined in eqn(31), versus ρ_c at $\beta = 6.2$ after 46 cools.

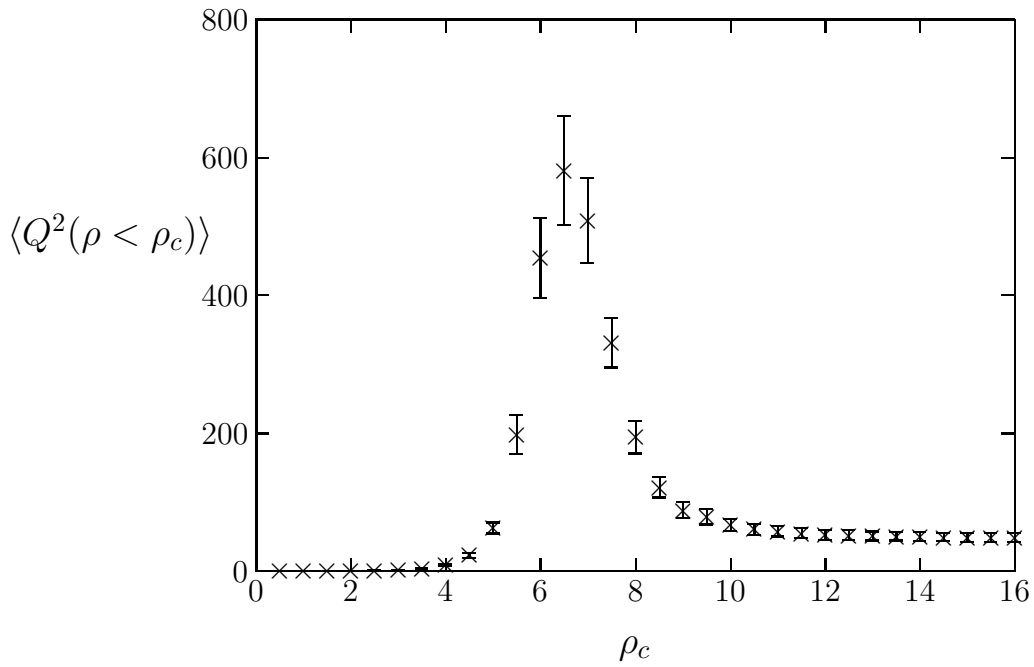


Figure 17: $\langle Q^2(\rho < \rho_c) \rangle$ against ρ_c at $\beta = 6.2$ after 23 cools.

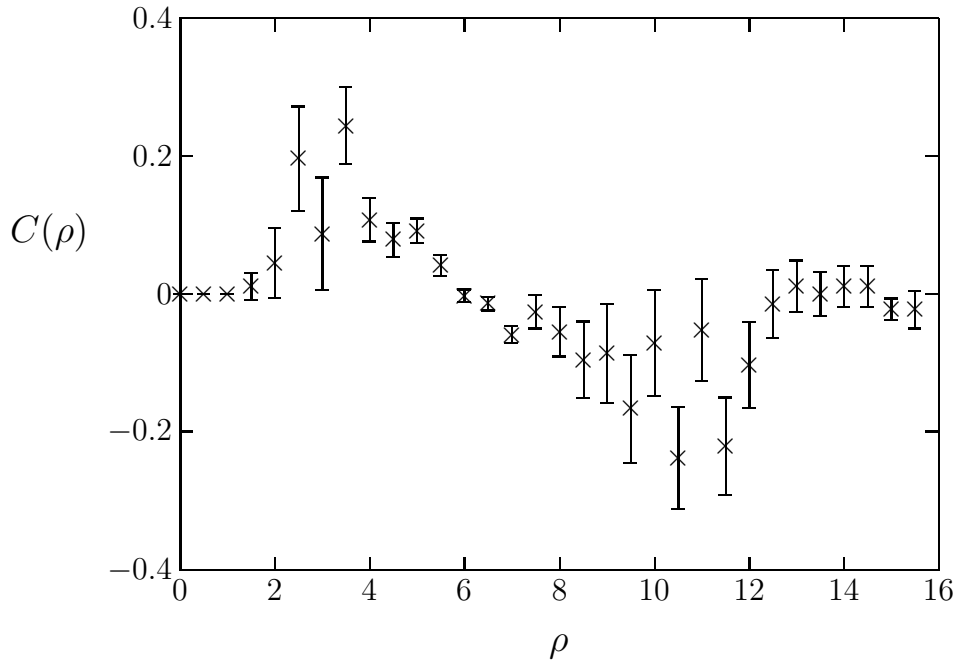


Figure 18: $C(\rho)$, as defined in eqn(32), versus ρ at $\beta = 6.2$ after 23 cools.

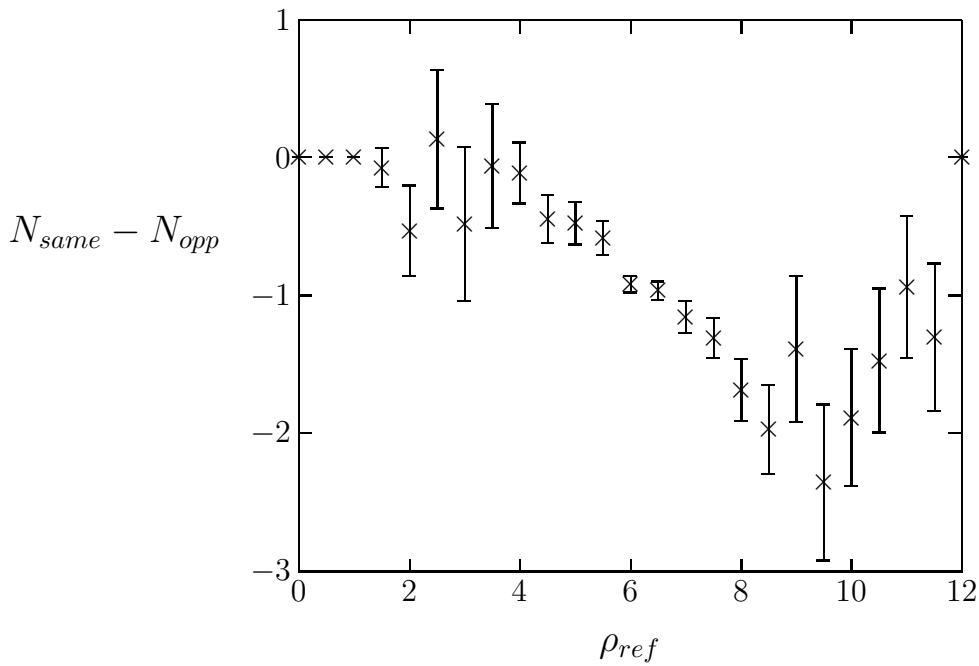


Figure 19: Net screening charge around a reference charge of size ρ_{ref} : at $\beta = 6.2$ after 23 cools.

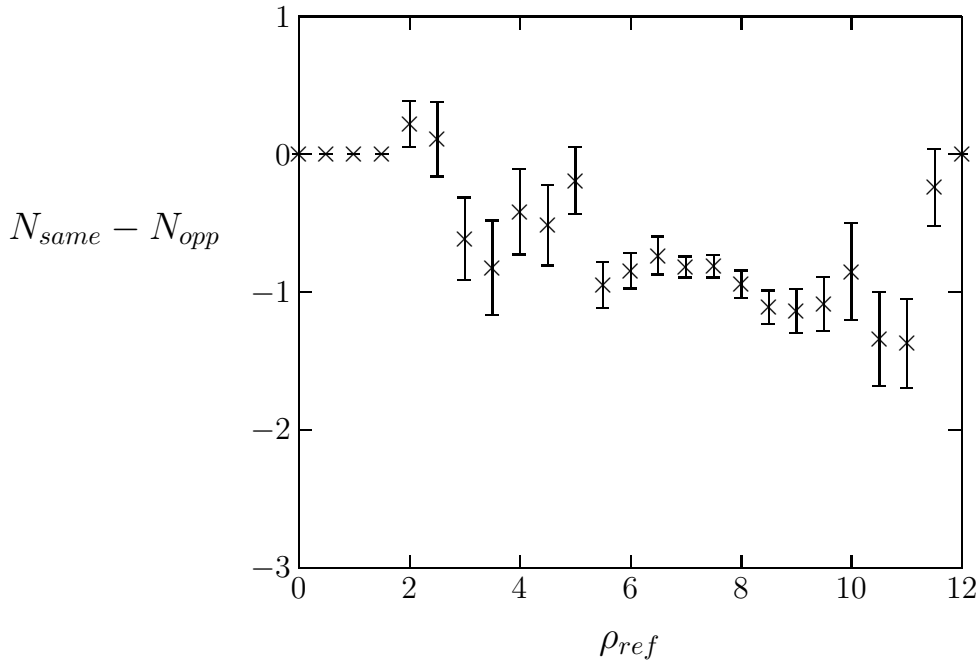


Figure 20: As in Fig 19 but after 46 cools.

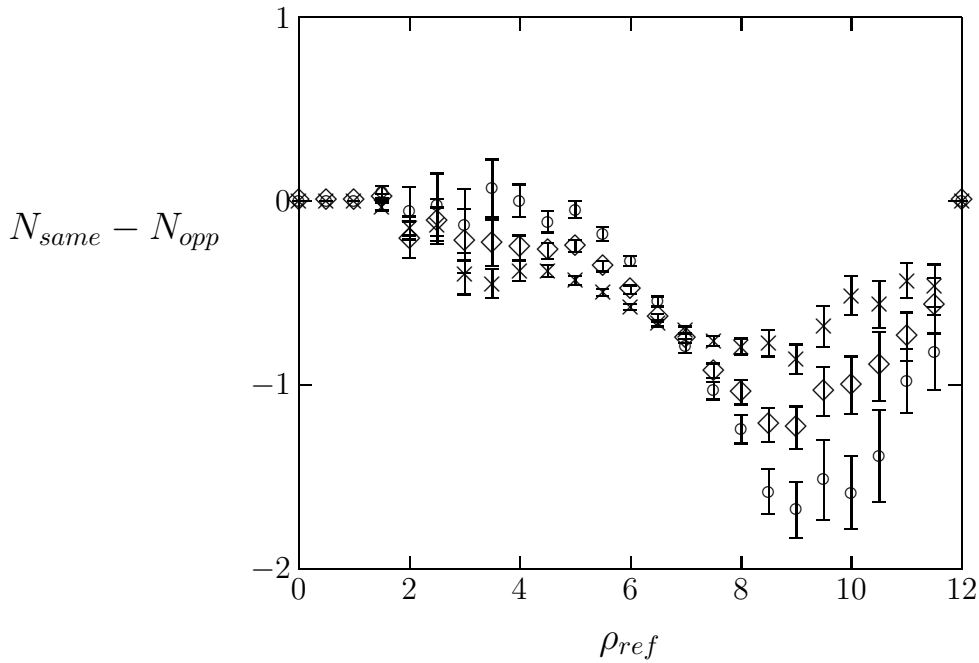


Figure 21: As in Fig 19, but only including screening charges with $\rho < 6$ and within a distance $R = 7(\times), 8(\diamond)$ or $9(\circ)$ of the reference charge.

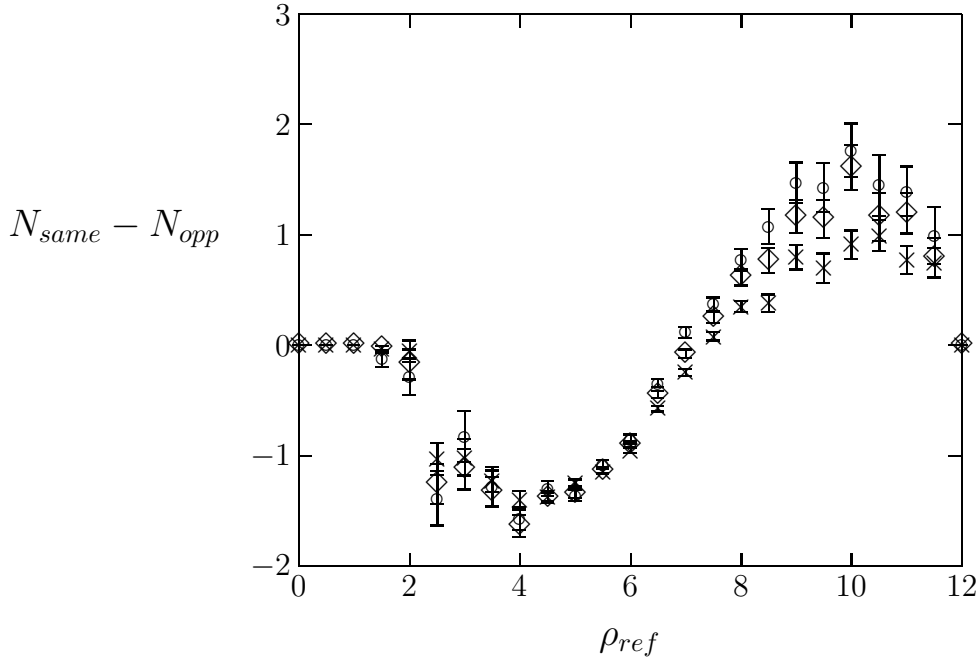


Figure 22: As in Fig 21, but only including charges with $\rho > 6$.

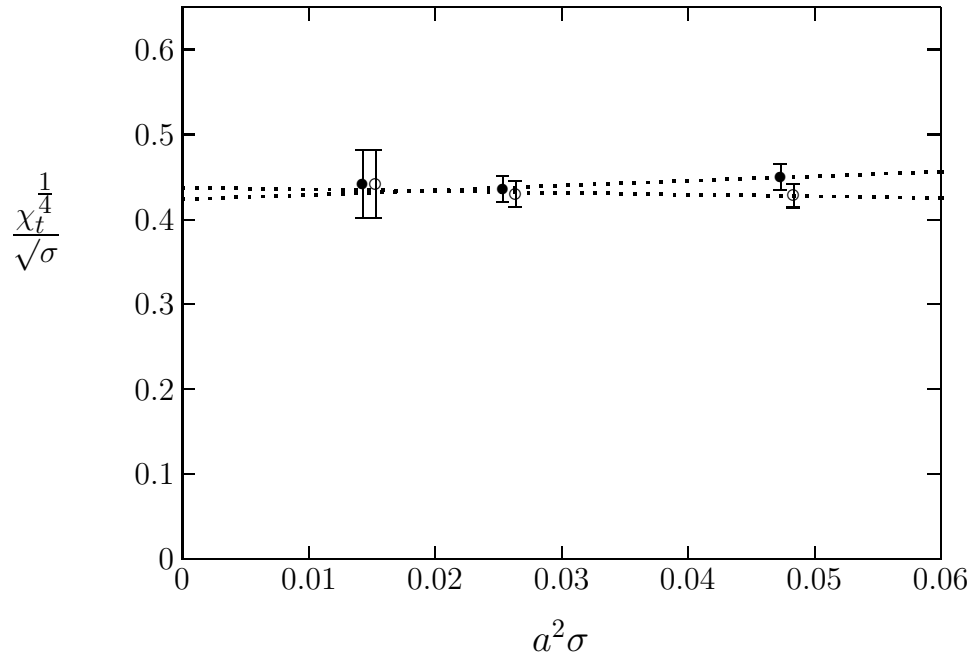


Figure 23: Plots of $\chi_t^{1/4}/\sqrt{\sigma}$ (•) and $\chi_{t,L}^{1/4}/\sqrt{\sigma}$ (o) against $a^2\sigma$ with continuum extrapolations.